



PNC

Piano nazionale per gli investimenti
complementari al PNRR

Ministero dell'Università e della Ricerca

FIT4MEDROB

D10.1.1

RTB1 - METHODS AND PROTOTYPES OF BIOHYBRID INTERFACES FOR NEUROREHABILITATION #1

Piano Nazionale Complementare (PNC) – Decreto Direttoriale n. 931 del 6 giugno 2022 – Avviso per la concessione di finanziamenti destinati ad iniziative di ricerca per tecnologie e percorsi innovativi in ambito sanitario e assistenziale

Initiative identifier: PNC0000007

Start date: 01/12/2022

Duration: 44 months

Website: www.fit4medrob.it

MLs: Loredana Zollo (UCBM), Fanny Ficuciello (UNINA)

ALs: Andrea Orlandini (CNR), Fabrizio Dabbene (CNR), Fanny Ficuciello (UNINA), Gionata Salvietti (UNISI), Loretta L. del Mercato (CNR), Paolo Netti (UNINA), Laura Pastorino (UNIGE)

Due date of deliverable: 30/11/2023

Actual submission date: 20/09/2024

Version: 1.1

DISSEMINATION LEVEL OF DELIVERABLE

PU	Public, fully open, e.g. web	X
CO	Confidential, restricted under conditions set out in Partners Agreement	



Ministero
dell'Università
e della Ricerca



Italiadomani
PIANO NAZIONALE
DI RIPRESA E RESILIENZA



PNC

Piano nazionale per gli investimenti
complementari al PNRR
Ministero dell'Università e della Ricerca



PNC

Piano nazionale per gli investimenti
complementari al PNRR

Ministero dell'Università e della Ricerca

HISTORY OF CHANGES

VERSION	SUBMISSION DATE	CHANGES
1.0	30/11/2023	First version
1.1	20/09/2024	Renaming of the Deliverable in light of the upcoming reorganization of the Deliverables/Objectives Introduction modified following reviewers' suggestions.



Ministero
dell'Università
e della Ricerca



Italiadomani
PIANO NAZIONALE
DI RIPRESA E RESILIENZA



PNC

Piano nazionale per gli investimenti
complementari al PNRR
Ministero dell'Università e della Ricerca

TABLE OF CONTENTS

History of Changes.....	2
1 RTb1 – Neurorehabilitation - Introduction	4
1.1 NEUROPTICSENS: Biosensing in human in vitro neurodegenerative processes	7
1.1.1 Sub-task 1.1 - Synthesis and calibration of pH sensors	8
1.1.2 Sub-task 1.2 - Application of sensors for intracellular pH sensing in 3D SH-SY5Y e M17 cultures	8
1.2 FUN-ROB: Functional nanop articles for biorobotics and rehabilitation.....	9
1.2.1 Sub-task 2.1 - Synthesis and characterization of MENPs.	10
1.2.2 Sub-task 2. - In silico assessment of MENPs.....	10
1.2.3 Sub-task 2.4 - In silico assessment of MENPs in hybrid scaffolds.....	10
1.2.4 Sub-task 2.7. - In silico MENPs peripheral nerve stimulation.....	10

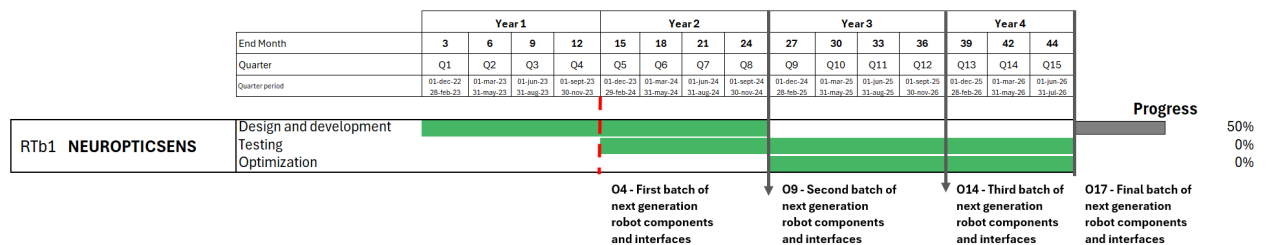
1 RTb1 – NEUROREHABILITATION - INTRODUCTION

Mission 3 is devoted to support **frontier research topics** pertaining to physical and computational aspects of robot *bodies*, robot intelligence, and interfaces with the patient. Seven research topics (RTa1...RTa4, RTb1..RTb3) are articulated in 19 sub-projects, running in parallel and covering complementary enabling technologies in the field of robotics and biorobotics.

In view of laying the foundations for the next wave of healthcare and personal care robots, this piece of research aims at gaining significant breakthroughs in the fields of (bio)materials interacting with human tissues. In this context, **Research Topic b1**, targets the clinical need of **Neurorehabilitation** and comprises of two complementary subprojects. More in detail the aim of RTb1 is to establish platforms for detecting disease-related biomarkers at the single cell level (sub-project#1 - **NEUROPTICSENS**), facilitating the screening and the administration of potential therapeutic compounds, and enabling remote cell stimulation (sub-project#2 - **FUNROB**). The target is represented by the central and peripheral nervous system. The platforms will be validated on advanced 3D human in vitro models of physiological and pathophysiological neuronal networks (Parkinson’s disease, PD).

NEUROPTICSENS progress

The timeline of NEUROPTICSENS is represented by the green lines in the Gantt below (Figure 1).

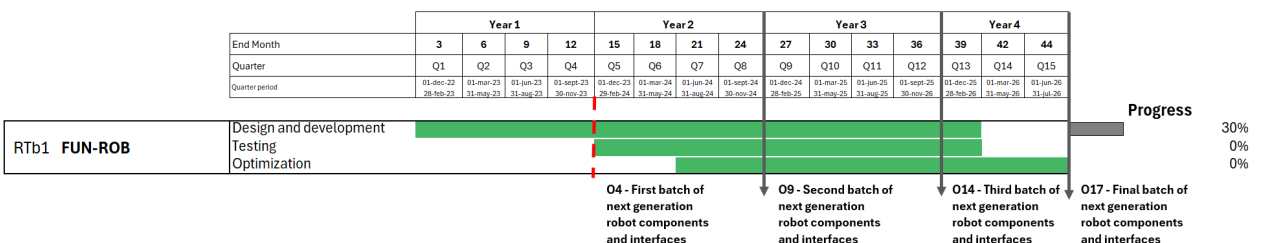


Specifically, “Design and Development” is referred to the synthesis, characterization and calibration of optical ratiometric pH microsensors and to the application of the microsensors for intracellular pH sensing in 3D cultures of two neuroblastoma cell lines, namely SH-SY5Y and 3K-SNCA (tasks 1.1, 1.2). The “**Design and Development**” phase is **50%** advanced compared to the planned Gantt. The microsensors have been synthesized and characterized and their in vitro cycompatibility on the two neuroblastoma cell lines has been preliminary characterized. The “**Testing**” (tasks 1.3, 1.4) phase “**Optimization**” one (task 1.5) have not yet started.

There are no deviations on the original plan and the research is progressing as originally foreseen.

FUNROB progress

The timeline of FUNROB is represented by the green lines in the Gantt below (Figure 2).

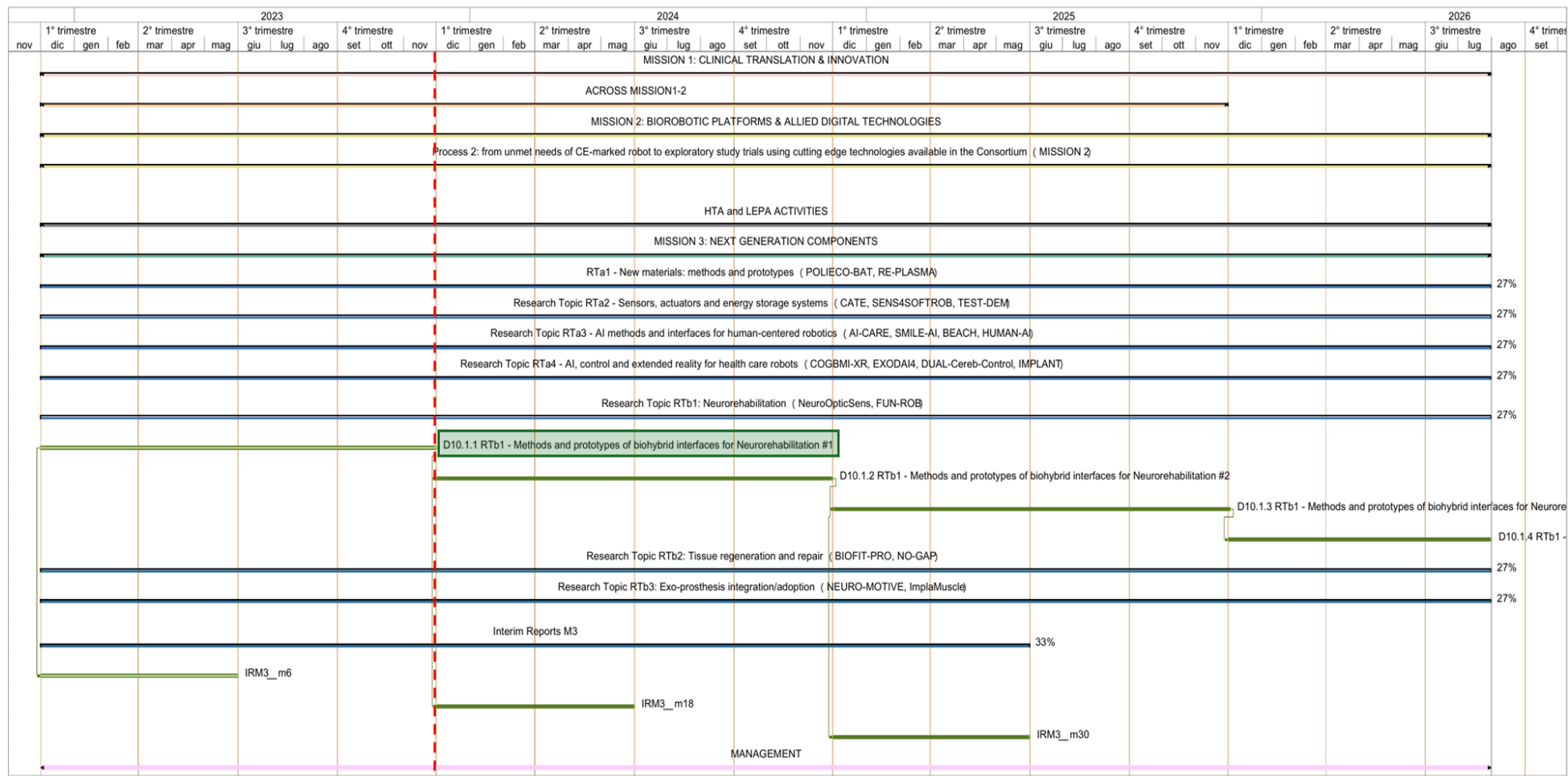


Specifically, “Design and Development” is referred to the synthesis and characterization of magnetoelectric nanoparticles MENPs, to the in-silico assessment of MENPs, to printing in hybrid scaffolds and to in silico assessment

of MENPs in hybrid scaffolds (tasks 2.1, 2.2, 2.3, 2.4). The “**Design and Development**” phase is **30%** advanced compared to the planned Gantt. The protocols for the synthesis of MENPs for remote stimulation at the single cell level have been defined, their silico modeling of magneto-electric behavior has been carried out and the computational simulation of magneto-electric nanoparticles dispersed in polymeric scaffolds has started. The “**Testing**” (tasks 2.5, 2.6, 2.7) phase and the “**Optimization**” one (tasks 2.8, 2.9) have not yet started.

There are no deviations on the original plan and the research is progressing as originally foreseen.

Overall, NEUROPTICSENS and FUNROB will contribute to Fit4MedRob by promoting the investigation of new hypotheses/ideas and technologies, including advanced in vitro platforms and nanoengineered smart (bio)materials, to overcome the main limits faced by current neurorehabilitation approaches.



2 NEUROPTICSENS: BIOSENSING IN HUMAN IN VITRO NEURODEGENERATIVE PROCESSES

This Section provides an overview of **NEUROPTICSENS** aiming at correlating the lysosomal-endolysosomal dysfunction to the electrophysiological activity of an advanced human based in vitro model of Parkinson's disease. A detailed description of **NEUROPTICSENS** is provided in the technical **Annex A**.

The dysfunction of the endolysosomal system has been demonstrated to play a central role in the pathogenesis of neurodegenerative diseases, specifically in Parkinson's disease [1]. A hallmark of PD is the aggregation of α -synuclein in the brain, α -synuclein is a cytosolic protein mainly found in the pre-synaptic terminals of neurons, where it is involved in synaptic neurotransmitter release and synaptic plasticity. Physiological α -synuclein can be degraded within lysosomes where enzymes work optimally at acidic pH. Abnormal lysosomal pH impairs lysosomal degradation affecting α -synuclein levels and aggregation. Once these aggregates are formed, they actively disrupt the processes of cellular trafficking and lysosomal clearance, allowing them to persist within neurons, leading ultimately to cellular self-destruction. Genes related to Parkinson's disease that disrupt mitochondrial function can result in the production of reactive oxygen species (ROS) or dopamine-o-quinone (DAQ), which can harm lysosomal machinery and, in turn, contribute to the formation of alpha-synuclein aggregates [2]. The aim of this subactivity is to correlate in vitro the lysosomal-endolysosomal dysfunction to the functional activity of PD advanced human models.

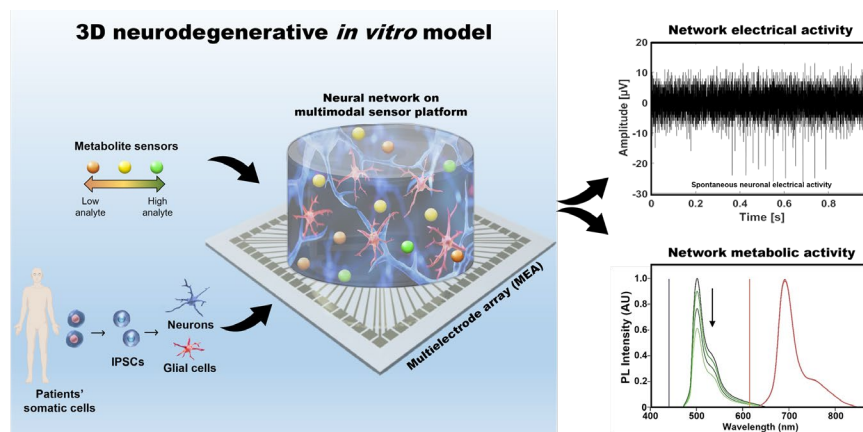


Fig. 1 - Graphical abstract of SubActivity#1

To reach this aim optical ratiometric pH-sensors, in combination with fully automated computational approaches, will be used to measure the acidification kinetics of endosomes and lysosomes in 3D human neural networks. The acidification kinetics will be correlated to the electrophysiological activity of the 3D networks recorded by microelectrode arrays. In **Figure 3** the graphical abstract of SubActivity#1 is shown. In this context 5 subtasks have been identified and are reported below with the indication of the involved participants:

- ST 1.1.** Synthesis and calibration of pH sensors (CNR).
- ST 1.2.** Application of sensors for intracellular pH sensing in 3D SH-SY5Y M17 cultures (UNIGE).
- ST 1.3.** Development and characterization of 3D in vitro human PD model (UNIGE).
- ST 1.4.** Application of sensors to 3D human PD model (UNIGE).
- ST 1.5.** Estimation of the acidification time in single living cells over time and space (CNR).

During the first 6 months of the project, the involved participants have been working on the definition of the main tasks and of their timing.

Starting from M6 to M12, the involved participants started working on subtasks 1 and 2, below the main results are reported.

2.1.1 Sub-task 1.1 - Synthesis and calibration of pH sensors

Optical sensors based on fluorescence allow *in situ*, 3D and real-time monitoring of intracellular acidification by monitoring the variation of fluorescence intensity caused by the variation of pH. Optical sensors can be employed without removing or damaging cells during culture, allowing thus the study of cell-cell interactions and the evaluation of their metabolic state. The sensors have been assembled employing a core inert material equipped with a sensing dye, selective towards protons changing, and a reference dye, adopted as internal standard, covalently linked onto the core material by means of chemical linkers. Silica has selected as inert core material since it doesn't have the tendency of interacting with cellular mechanisms, and thus it does not interfere with their study [3]. Moreover, silica can be produced in a wide range of monodispersed materials with different shapes, sizes and wettability thanks to its simple method of synthesis, low cost, its eco and biocompatibility [4]. During this period, the protocols for the synthesis of the optical ratiometric pH-sensors have been optimized and the sensors have been characterized. Namely, highly stable optical ratiometric pH-sensors based on silica microparticles have been synthesized via a modified Stoeber method [5] and fully characterized by means of dynamic scattering, spectrofluorimetric analyses, electron, and fluorescence microscopy.

2.1.2 Sub-task 1.2 - Application of sensors for intracellular pH sensing in 3D SH-SY5Y e M17 cultures

SH-SY5Y cell line and M17 with 3K mutation on alpha-synuclein gene (3K-SNCA) have been used for the experiments carried out during this period. Specifically, *in vitro* models of Parkinson's disease (PD) need to replicate the two primary pathological features of the condition: the degeneration of dopaminergic neurons and the intraneuronal accumulation of alpha-synuclein [6]. The most adopted *in vitro* model for PD involves the cultivation of immortalized cell lines [7]. This *in vitro* model is prevalent, readily accessible, cost-effective, and can serve as an initial stage for investigating the disease mechanisms or potential interventions. Among the immortalized cell lines used for this topic, human-derived SH-SY5Y cell line is the most employed in this research field. SH-SY5Y is a cell subline derived from a metastatic neuroblastoma in a 4-year-old female's bone marrow [8]. Furthermore, SH-SY5Y can be induced to differentiate into a more mature dopaminergic phenotype [9]. Given these attributes, this cell line represents a suitable *in vitro* model for studying PD. In addition, M17 cells represents another type of immortalized cell line widely used in PD *in vitro* models expressing 3K mutation on alpha-synuclein gene. During this period, the differentiation of 3K-SNCA cells in 2D and the application of pH-sensors on 2D cultures was carried out. Specifically, both the culture protocols and the differentiation ones have been developed for SH-SY5Y and M17 neuroblastoma huma cells. The results showed that both cell lines nearly completed their differentiation within 10 days. Namely, at the first day *in vitro* (DIV 0), the cells did not express the neuronal marker (MAP2), but only the protein α -synuclein, whereas a high expression of MAP2 was observed at DIV10 indicating the differentiation into neuron-like cells. For the preliminary biocompatibility tests with pH-sensors, SH-SY5Y cells were observed at 4h and 48h after the exposition to pH-sensors. Images were taken in green and red fluorescence and transmission channels. The overlay of the three channels showed clear evidence of absence of cytotoxicity since cell proliferation was not affected by the sensors. Furthermore, it was evident the correlation among the colour changes of the sensors and the changes in pH values.

3 FUN-ROB: FUNCTIONAL NANOPARTICLES FOR BIROBOTICS AND REHABILITATION

This Section provides an overview of **FUN-ROB** aiming at developing active nanomaterials for the non-invasive stimulation of the peripheral nervous system. A detailed description of **FUN-ROB** is provided in the technical **Annex B**. Multiferoic magneto-electric nanoparticles (MENPs) are colloidal inorganic nanoparticles with a very interesting potential in nanomedicine, spintronics, and electrocatalysis [10-12]. Owing to the existence of the magneto-electric (ME effect), an intrinsic coupling between magnetic and electric fields occurs in these materials. Generally, such hetero-structured materials consist of a magnetostrictive domain which converts a magnetic field into a vibrational lattice strain, and a piezoelectric domain which converts the strain generated at the heterointerface (the coupling area) into an electric field. This electric field induces also the formation of charge carriers. High values of ME voltage coefficients express the efficiency of energy conversion from magnetic field to electricity. The possibility of eliciting high amplitude electric fields when stimulated wirelessly by small amplitude magnetic fields opens a wide range of applications in the biomedical domain, and for the modulation of the nervous system activity. Using MENPs it is possible to obtain single-neuron spatial resolution coupled with minimal energy dissipation and remote activation and control through a safe magnetic source. These characteristics could play a crucial role in the modulation and stimulation of the peripheral nervous system, considering the increasing interest in new stimulation techniques, less invasive but with higher selectivity that had a rapid development in prosthetic technologies to achieve sensory feedback control with desirable high spatial and temporal resolution. This subactivity aims at realizing active nanomaterials for the stimulation of the peripheral nervous system with applications in the field of neurorehabilitation, as depicted in **Figure 4**.

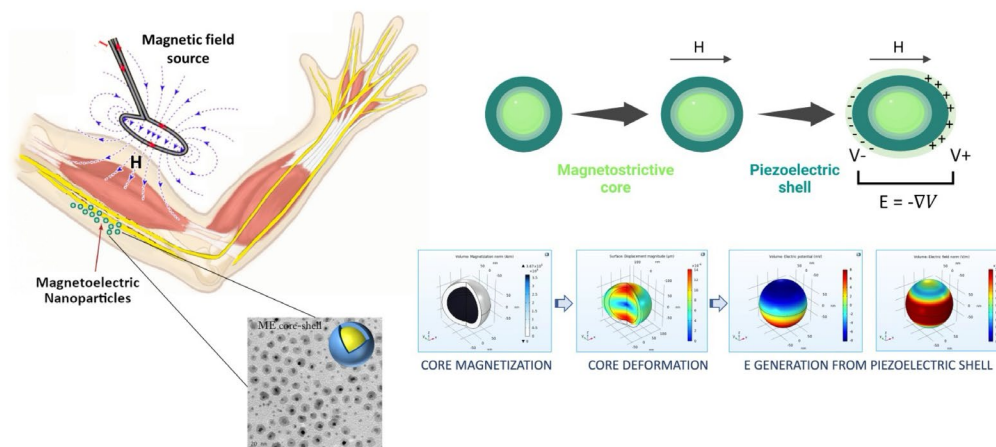


Fig. 2 - Graphical abstract of SubActivity#2.

ME heterostructured colloidal nanoparticles, i.e., nanosized core-shell magneto-electric materials, will be engineered and suitably incorporated within biocompatible hybrid scaffolds, for the selective stimulation of nerve fibres at the interface with prosthetic systems. The as-developed hybrid materials will be characterized through *in silico* approaches and *in vitro* experiments; the development and handling of such materials will offer the possibility of overcoming the limitations of current peripheral nerve stimulation techniques, offering a completely new and versatile tool in terms of spatial and temporal resolution and controllability of interface phenomena opening new numerical simulations have been identified and are reported below with the indication of the involved participants:

- ST 2.1. Synthesis and characterization of MENPs (CNR NANOTEC).
- ST 2.2. *In silico* assessment of MENPs (CNR IEIIT).
- ST 2.3. Printing in hybrid scaffolds (CNR NANOTEC).
- ST 2.4. *In silico* assessment of MENPs in hybrid scaffolds (CNR IEIIT).
- ST 2.5. Magnetic sources (CNR IEIIT).
- ST 2.6. MagnetoElectric coupling measurements (CNR NANOTEC, UniSalento).

ST 2.7. *In silico* MENPs peripheral nerve stimulation (CNR IEIIT).

ST 2.8. *In vitro* experiments. (CNR NANOTEC, UniGenova).

ST 2.9. *In vivo* experiments (to be assigned, likely via cascade calls).

3.1.1 Sub-task 2.1 - Synthesis and characterization of MENPs.

This Task is focused on preparative methodologies developed by CNR NANOTEC for the liquid-phase chemical synthesis of MENPs with controlled structural (crystalline phase), geometrical (size, morphology), and surface (protective "capping" molecules) characteristics that can be precisely correlated with experimental process parameters (temperature, concentration and relative ratio of reagents, synthesis technique). The synthetic protocols derived from the literature for the preparation, extraction, and purification of NPs of Fe₃O₄ and Co_xFe_{3-x}O₄ with isotropic geometries have been optimized on the typical scale of a research chemical laboratory, equipped with state-of-the-art equipment. Specifically, the synthesis of magnetic NPs via thermal decomposition in an organic ambience (solvothermal) either occurring via μ W approaches or in a reaction flask (Schlenk line) has been carried out. Morphological, structural, compositional, and magnetic characterization tests/analyses are in progress.

3.1.2 Sub-task 2. - In silico assessment of MENPs.

The *in-silico* assessment has been based on the most widely used configuration of MENPs, i.e. the core-shell system based on CoFe₂O₄ (Cobalt Ferrite, CFO, spinel structure)—BaTiO₃ (Barium Titanate, BTO, perovskite structure). The magnetoelectrical behaviour, in terms of ME coupling coefficient (α_{ME}), of core-shell MENPs with different shapes has been analysed through a numerical model. The nanostructures have been initially subjected to a high-amplitude DC magnetic field to assess their electrical output. Moreover, a following study has been performed under a time-variant and low amplitude magnetic field at low frequency (50 Hz), as several recent works reported how this type of magnetic stimulation commonly adopted for biomedical applications can yield an improved ME response.[13-16] Results of this study pinpoint the possibility of efficiently modulating the MENPs' electrical output also by varying their geometrical features, an approach less investigated so far. Overall, the obtained results have shown that MENPs with a more elongated morphology exhibit a superior ME coefficient if compared with spherical nanoparticles of similar volume, for both DC and AC magnetic fields. This response is due to the presence of a larger surface area at the interface between the magnetostrictive core and piezoelectric shell, and to the MENP geometrical orientation along the direction of the magnetic field. Moreover, the locally induced electrical field becomes drastically enhanced under the low amplitude AC field if the material has been pre-magnetized, leveraging on the "memory effect" of the core hysteretic behaviour. The herein presented concept can be broadened to engineer various geometrical interphase configurations, thus gaining fundamental knowledge to support MENPs synthesis.

3.1.3 Sub-task 2.4 - In silico assessment of MENPs in hybrid scaffolds.

The task started its activities, by the identification of the main mechanical and dielectric properties of those polymers that (1) can be processed via the conventional fabrication techniques and (2) can be at the basis of the hybrid scaffold in which ME nanostructures will be printed. By using a multiphysics approach like the one reported for task 2, preliminary computational simulations have been carried out to assess the feasibility of this approach, and the influence of the number of the ME nanostructures within a unit reference of the model, as well as their positioning within the polymeric matrix.

3.1.4 Sub-task 2.7. - In silico MENPs peripheral nerve stimulation

The most promising approach for *in silico* assessment of the interaction between MENPs printed in hybrid scaffolds and the peripheral nervous system has been identified, as well as the most suitable models of neuronal dynamics. Preliminary results have been obtained by considering a few MENPs not printed in a hybrid scaffold but hypothesized to be placed at different positions in the proximity of peripheral nerves, highlighting, as expected, a great influence of the distance between the MENPs and the nerve fibre on the elicited response.



Piano Nazionale Complementare (PNC) – Decreto Direttoriale n. 931 del 6 giugno 2022 – Avviso per la concessione di finanziamenti destinati ad iniziative di ricerca per tecnologie e percorsi innovativi in ambito sanitario e assistenziale

Project identifier: PNC0000007

Start date: 01/12/2022

Duration: 44 months

Website: www.fit4medrob.it

ACTIVITY 10– BIOHYBRID INTERFACES AND BIOMATERIALS

SUBACTIVITY#1

RESEARCH TEAMS PERIODIC REPORT, M1-M12

PI: Di Lisa Donatella (UNIGE), Onesto Valentina (CNR)

Partner Acronym: UniGenova, CNR NANOTEC

Date: 01/11/2023

TABLE OF CONTENTS

1	<i>Deliverables worked on during this period.....</i>	3
2	<i>Subactivity#1: Biosensing In Human In Vitro Neurodegenerative Processes</i>	3
2.1	<i>Achievements</i>	5
3	<i>Dissemination activities (scientific papers, pop magazines, tv, etc.)</i>	10
4	<i>Meetings in this period</i>	11
5	<i>Recruitment in this period</i>	12
	<i>References</i>	12

1 DELIVERABLES WORKED ON DURING THIS PERIOD

- D 10.1 – Subactivity#1: *Biosensing in human in vitro neurodegenerative processes*

2 SUBACTIVITY#1: BIOSENSING IN HUMAN *IN VITRO* NEURODEGENERATIVE PROCESSES

This section provides an overview of SubActivity#1, which is focused on the biosensing in human *in vitro* neurodegenerative processes. It includes the driving concept, the work plan, the identified sub-tasks, and the groups involved. To facilitate a clearer understanding of each group's expertise and contribution, several one-on-one meetings have been conducted. Additionally, group meetings have been held to establish collaborations and delineate the sub-activities.

Rationale. The endolysosomal system is vital for the function and survival of neurons, mediating local trafficking in synapses and dendrites, while also communicating with the soma to integrate signalling pathways and the turnover of organelles and macromolecules originating in this distinct and distant compartments [1]. Genetic studies, the dissection of biochemical pathways and rapidly evolving techniques for live cell imaging are increasingly implicating deficits in the endolysosomal system in the pathogenesis of neurodegenerative diseases such as Alzheimer's disease (AD), Parkinson's disease (PD) and amyotrophic lateral sclerosis (ALS) [1]. The formation of autophagosomes in distal axons and synapses and their retrograde transport back to the soma for fusion with lysosomes are impaired in AD, PD and ALS. Evidence of dysfunction of the endolysosomal system playing a central role in disease pathogenesis is strongest in PD. The identification of various genes linked to Parkinson's disease has brought attention to essential cellular pathways crucial for its development [2]. The genetic variations associated with both idiopathic and familial Parkinson's disease are categorized based on their respective cellular pathways and functions, **Figure 1**. A hallmark pathology of PD is α -synuclein aggregation in the brain. α -synuclein is a cytosolic protein mainly found in the pre-synaptic terminals of neurons, where it is involved in synaptic neurotransmitter release and synaptic plasticity. Physiological α -synuclein can be degraded within lysosomes where enzymes work optimally at acidic pH. Abnormal lysosomal pH impairs lysosomal degradation affecting α -synuclein levels and aggregation. In particular, once these aggregates are formed, they actively disrupt the processes of cellular trafficking and lysosomal clearance, allowing them to persist within neurons and ultimately leading to cellular self-destruction. Genes related to Parkinson's disease that disrupt mitochondrial function can result in the production of reactive oxygen species (ROS) or dopamine-o-quinone (DAQ), which can harm lysosomal machinery and, in turn, contribute to the formation of alpha-synuclein aggregates [2].

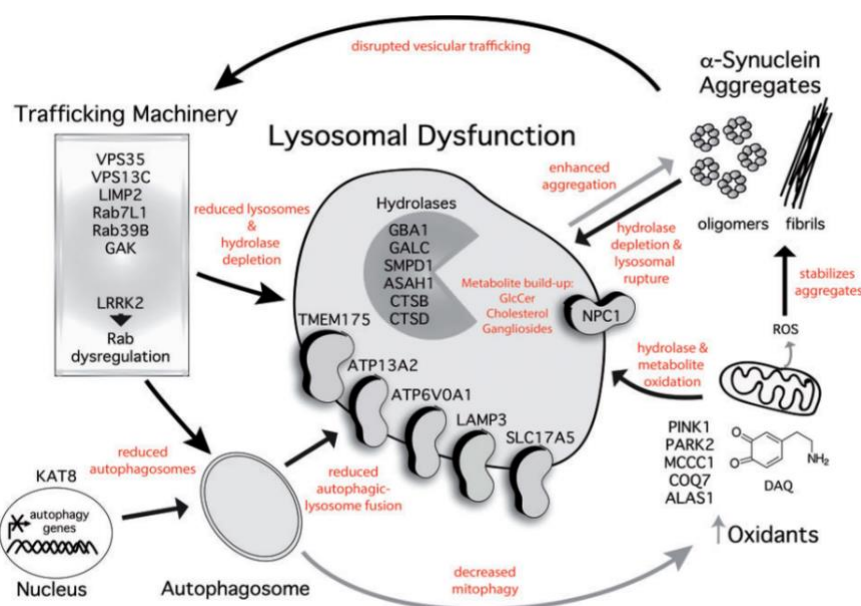


Figure1. Parkinson's disease as a complex genetic disorder that converges on lysosomal dysfunction [2].

Aim. The final goal of this subactivity is focused on the correlation of lysosomal-endolysosomal dysfunctions and functional activity to neurodegenerative diseases, specifically to PD in advanced human *in vitro* models, **Figure 1**.

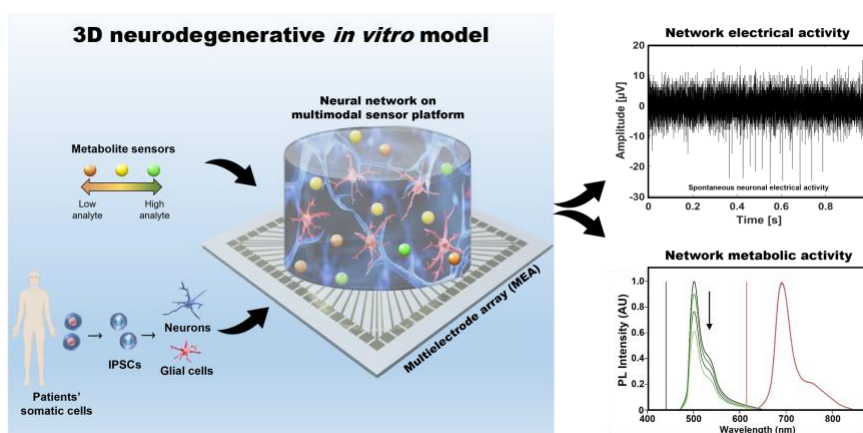


Figure1. Graphical abstract of Subactivity#1

Methods. Application of highly stable optical ratiometric pH-sensors, in combination with fully automated computational approaches, for precisely measuring the acidification kinetics of endosomes and lysosomes in 3D human neural networks. The acidification kinetics will be correlated to the electrophysiological activity of the 3D networks recorded by microelectrode arrays.

Subtasks:

ST1.1 Synthesis and calibration of pH sensors (CNR): Highly stable optical ratiometric pH-sensors based on silica microparticles will be synthesized via a modified Stober method and fully characterized by means of dynamic scattering, spectrofluorimetric analyses, electron, and fluorescence microscopy. The pH sensors will be then added to

2D SH-SY5Y and M17 cell cultures, bearing PD mutation for α -synuclein aggregation, and to 2D human PD and healthy neurons. Their internalization and co-localization with endosomes and lysosomes will be studied by means of FACS and fluorescence microscopy analyses.

ST1.2 Application of sensors for intracellular pH sensing in 3D SH-SY5Y and M17 cultures (UNIGE): As a first step, 3D models of PD will be developed using SH-SY5Y and M17 cell lines to optimize the protocol for the intracellular pH sensing before its use with human derived models.

ST1.3 Development and characterization of 3D in vitro human PD model (UNIGE): A 3D *in vitro* model of PD will be developed by encapsulating neurons, differentiated from patient derived induced pluripotent stem cells, and astrocytes into a hydrogel recapitulating the main physico-chemical characteristics of the brain extra cellular matrix. The model will be characterized morphologically, by immunocytochemistry techniques, and functionally, using by microelectrode arrays to record over time its spontaneous electrophysiological activity. Obtained data will be compared to those obtained for 3D human models derived from healthy donors to underline significant differences in activity patterns.

ST1.4 Application of sensors to 3D human PD model (UNIGE): The developed pH sensor will be applied both to the 3D human PD and healthy neuronal networks and the acidification kinetics will be correlated to their functional activity. Candidate drugs, such as ambroxol, will be tested respect to their impact on lysosomal activity and network functionality.

ST1.5 Estimation of the acidification time in single living cells over time and space (CNR): The pH-sensor read-out will be quantified by applying a fully automated computational approach for precisely measuring the acidification kinetics of endosomes and lysosomes in the neural networks over space and time.

The involved groups in Subactivity#1 are the CNR Nanotec (Institute of Nanotechnology), Lecce, and the Dept. Informatics, Bioengineering, Robotics and Systems Engineering (DIBRIS), University of Genoa, Genoa.

The following people have been involved in defining the sub-tasks:

- Dr. Loretta L. del Mercato (CNR)
- Dr. Valentina Onesto (CNR)
- Dr. Helena Luele (CNR)
- Dr. Stefania Forciniti (CNR)
- Prof. Laura Pastorino (UNIGE)
- Prof. Sergio Martinoia (UNIGE)
- Prof. Michela Chiappalone (UNIGE)
- Dr. Donatella Di Lisa (UNIGE)
- Dr. Andrea Andolfi (UNIGE)
- Dr. Valentina Pavanati (UNIGE)

2.1 ACHIEVEMENTS

The main achievements of this period are:

- (i) definition of the work plan and partners identifications.
- (ii) preliminary results related to *Subtasks 1.1 and 1.2*.

- **Work plan**

Five subtasks have been developed, as already reported in section 2. During the first 6 months of the project, the involved groups defined for each subtask, specific activities, developing a Gantt diagram, **Figure 2**.

From M6 to M12, the groups started to work on *Subtasks 1.1 and 1.2*.

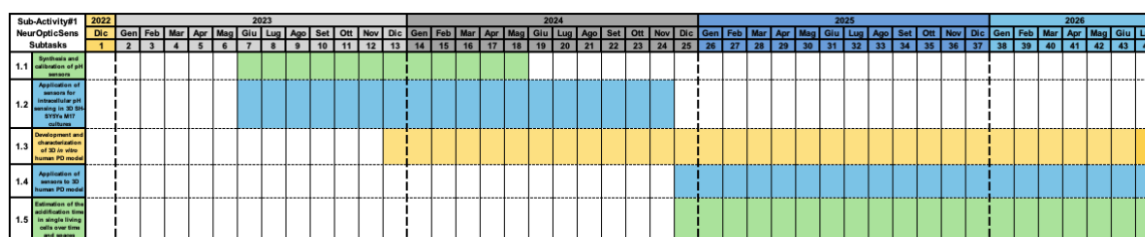


Figure 2. Gantt diagram of Subactivity#1.

- **Subtasks 1.1 - Synthesis and calibration of pH-sensors**

Optical sensors based on fluorescence allow *in situ*, 3D, real-time monitoring of acidification basing on the changes of fluorescence intensity caused by pH variations. Optical sensors can be employed without removing or damaging cells during culture, allow to study of cell-cell interactions and to evaluate their metabolic state.

This subtask involved two different activities:

1. Synthesis of optical ratiometric pH-sensors (6 months)
2. Characterization and calibration of the pH-sensors (6 months)

Preliminary results:

During this period (M6-M12), the activity was focused on the synthesis of optical ratiometric pH-sensors.

Methods:

Optical ratiometric pH-sensors in the micrometric range were synthesized by a bottom-up approach (**Figure 3**).

Specifically, they were assembled employing a core inert material equipped with a sensing dye, selective towards protons changing, and a reference dye, adopted as internal standard, covalently linked onto the core material by means of chemical linkers. Silica was selected as inert core material since it doesn't have the tendency of interacting with cellular mechanisms, and thus it does not interfere with their study [3]. Moreover, silica can be produced in a wide range of monodispersed materials with different shapes, sizes and wettability thanks to its simple method of synthesis, low cost, its eco and biocompatibility [4].

Silica core particles, with uniform diameter, were further functionalized with a shell of biocompatible hydrogel to improve their dispersion in aqueous media ensuring a homogeneous sensors distribution an effective 3D pH mapping in culture cells and to simultaneously link the Fluorescein-5-isothiocyanate (FITC) and Cyanine3 NHS Ester (Succinimidyl Ester) (CY3) selected as sensing and reference dyes, respectively, for the pH monitoring.

Briefly, silica seeds (**Figure 3a**) were synthesized adopting a modified Ströeber protocol [5] employing the tetraethyl orthosilicate (TEOS) as monomer and carrying out the reaction under stirring at room temperature for 20 minutes. After that, the silanization was carried out for 24 hours at room temperature under stirring, injecting into the silica particles flask a mixture of 3-(Trimethoxysilyl) propyl methacrylate (MPS) linker and TEOS dissolved in ethanol (**Figure 3b**). Once the silanization reaction was completed more ethanol and ammonium persulfate (APS) were added to the flask and the temperature was raised to 60 °C. A mixture of 2-Aminoethylmethacrylamide hydrochloride (AEMA) and N,N,N',N'-Tetramethyl ethylenediamine (TEMED) catalyst dissolved in EtOH were injecting into the silica particles flask for 1 hour at 60°C under stirring in order to polymerize an hydrogel layer around the silanized silica core (**Figure 3c**). The reaction was stopped centrifuging the flask mixture and the precipitated microparticles were recovered. SiO₂ core-shell microparticles were further washed with ethanol. As the last step, the coupling reaction with the sensing and reference dyes was realized for 24 hours at room temperature under stirring, dissolving FITC and CY3 in ethanol and adding SiO₂ core-shell MPS-AEMA microparticles to the mixture (**Figure 3d**). SiO₂ core-shell MPS-AEMA-FITC/CY3 microsensors were washed in ethanol and stored again in ethanol at room temperature in the dark.

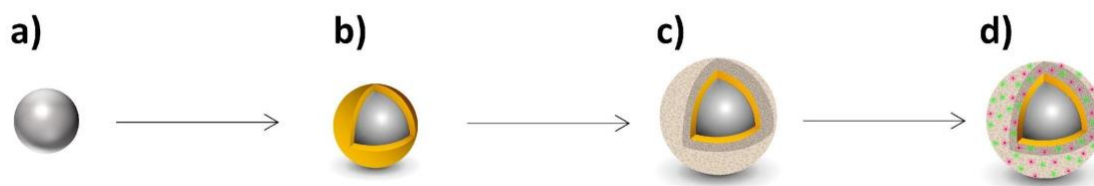


Figure 3. Schematic representation of the synthesis steps for the fabrication of optical ratiometric pH-sensors. a) Silica core formation, b) silanization with a linker, c) polymerization of the hydrogel layer around the silanized silica core, d) covalent link of the pH sensing (green) and reference (red) dyes.

• **Subtask 1.2 - Application of sensors for intracellular pH sensing in 3D SH-SY5Y e M17 cultures**

SH-SY5Y cell line and M17 with 3K mutation on alpha-synuclein gene (3K-SNCA) were used for the experiments carried out during this period (M6-M12). Specifically, *in vitro* models of Parkinson's disease (PD) need to replicate the two primary pathological features of the condition: the degeneration of dopaminergic neurons and the intraneuronal accumulation of alpha-synuclein [6]. The most commonly adopted *in vitro* model for PD involves the cultivation of immortalized cell lines [7]. This *in vitro* model is prevalent, readily accessible, cost-effective, and can serve as an initial stage for investigating the disease's underlying mechanisms or potential interventions [6], [7]. Among the immortalized cell lines used for this topic, human-derived SH-SY5Y cell line is the most commonly employed in this research field. SH-SY5Y is a cell subline derived from a metastatic neuroblastoma in a 4-year-old female's bone marrow [8]. Furthermore, SH-SY5Y can be induced to differentiate into a more mature dopaminergic phenotype [9]. Given these attributes, this cell line serves as a suitable *in vitro* model for studying PD. In addition, M17 cells represents another type of immortalized cell line widely used in PD *in vitro* models expressing 3K mutation on alpha-synuclein gene tagged. Both cell lines have been provided by the Schapira Lab (UCL, London).

This subtask involved two different activities:

1. Differentiation of SH-SY5Y and 3K-SNCA cells in 2D (1 months)
 - a. Application of the pH sensors on 2D cultures (6 months)
2. Differentiation of SH-SY5Y and 3K-SNCA cells in 3D (6 months)
 - a. Applications of the pH sensors in 3D cultures (6 months)

During this period, the activity was focused on the differentiation of 3K-SNCA cells in 2D and the application of pH-sensors on 2D cultures.

Methods:

1. *Differentiation of SH-SY5Y and 3K-SNCA cells in 2D (1 months)*

Differentiation protocols have been developed for both SH-SY5Y and M17 neuroblastoma huma cells.

Neuroblastoma human cells SH-SY5Y:

Neuroblastoma human cells SH-SY5Y were provided in frozen vials. After thawing, the cells were seeded into two T-75 flasks containing pre-warmed culture medium at 37°C. The culture medium consists of DMEM/F:12, 1% Glutamax, 1% Pen/Strep and 10% fetal bovine serum (FBS). The cells were then placed in an incubator at 37°C with 5% CO₂ and 95% humidity until they reached 80% confluence.

Neuroblastoma human cells M17 cells with 3K-SNCA mutation:

Neuroblastoma human cells M17 cells with 3K mutation on alpha-synuclein gene were provided in frozen vials. After thawing, the cells were seeded into two T-75 flasks containing a pre-warmed culture medium at 37°C. The culture medium consists of DMEM, 1% Glutamax, 1% Pen/Strep and 10% fetal bovine serum (FBS). The cells were then placed in an incubator at 37°C with 5% CO₂ and 95% humidity until they reached 80% confluence.

Differentiation protocol:

The differentiation protocol developed for both SH-SY5Y and M17 cells involved the use of retinoic acid (RA) and brain-derived neurotrophic factor (BDNF) for at least 10 days. Specifically, petri-dishes (ø 35mm) were coated with

a poly-ornithine solution (0.1 mg/ml) for 1 hour at room temperature, then washed with 1 ml of DPBS and subsequently, coated with 1 ml of laminin solution (1 µg/ml). Before seeding, laminin solution was removed.

Undifferentiated cells are detached using 0.25% trypsin. Cells were centrifuged at 1000 rpm for 10 minutes. The pellet was resuspended in 1 ml of differentiation medium composed of Neurobasal medium with 0.5% B27 supplement, 30 µM retinoic acid, 1% Glutamax, 1% Pen/Strep and 10 ng/ml BDNF. Cells were plated with a cell density of 800 cells/mm² on the pre-coated petri-dishes. Cell cultures were maintained in incubator at 37°C in a controlled environment with a 5% CO₂ concentration and 95% humidity. Complete Neurobasal medium has been changed every 2 or 3 days, minimizing exposure to light and limiting microscope exposure time since retinoic acid is light-sensitive.

Samples were fixed for immunocytochemical characterization at DIV 0 and DIV 10. To assess the expression of specific neuronal markers, both cells were fixed in 4% paraformaldehyde in phosphate buffer solution (PBS), pH 7.4 for 30 min at room temperature. Permeabilization was achieved with PBS containing 0.1% Triton-X100 for 10 min at room temperature and non-specific binding of antibodies was blocked with an incubation of 45 min in a blocking buffer solution consisted of PBS, 0.3% bovine serum albumin (BSA) and 0.5% FBS. Cultures were incubated with primary antibody diluted in PBS Blocking buffer for 1 h at room temperature. Cultures were rinsed three times with PBS and finally exposed to the secondary antibodies. The following primary antibodies were used: MAP-2 (1:500) as neuronal marker, Michael J. Fox (1:200) as α-synuclein marker, Dapi (1:10000) for nuclei. Cultures were rinsed twice with PBS and finally exposed to the secondary antibodies: Alexa Fluor 488, Alexa Fluor 549, Alexa Fluor 633 Goat anti mouse or Goat anti rabbit, diluted 1:700 and 1:1000.

a. Application of the pH sensors on 2D cultures (6 months)

Preliminary biocompatibility tests were carried by exposing the SH-SY5Y cells to the pH sensors. Specifically, 1 µL of SiO₂ FITC/CY3 stock solution has been added in 1 ml of differentiation medium and 10 µL of SiO₂ FITC/CY3 diluted in differentiation medium was added in the samples. An Olympus BX-51 upright microscope was used for immunofluorescence evaluation of the biological samples and the image acquisition was done with a Hamamatsu Orca ER II digital cooled CCD camera driven by Image ProPlus software (Media Cybernetic).

Preliminary results:

Both the SH-SY5Y and 3K-SNCA cell lines have nearly completed their differentiation within 10 days, as indicated in **Figure 4**. Specifically, it's noticeable that at DIV 0, the cells did not express the neuronal marker (MAP2), but only the α-synuclein, a protein that abnormally aggregates in the brain tissue affected by Parkinson's disease, **Figure 4A-B**.

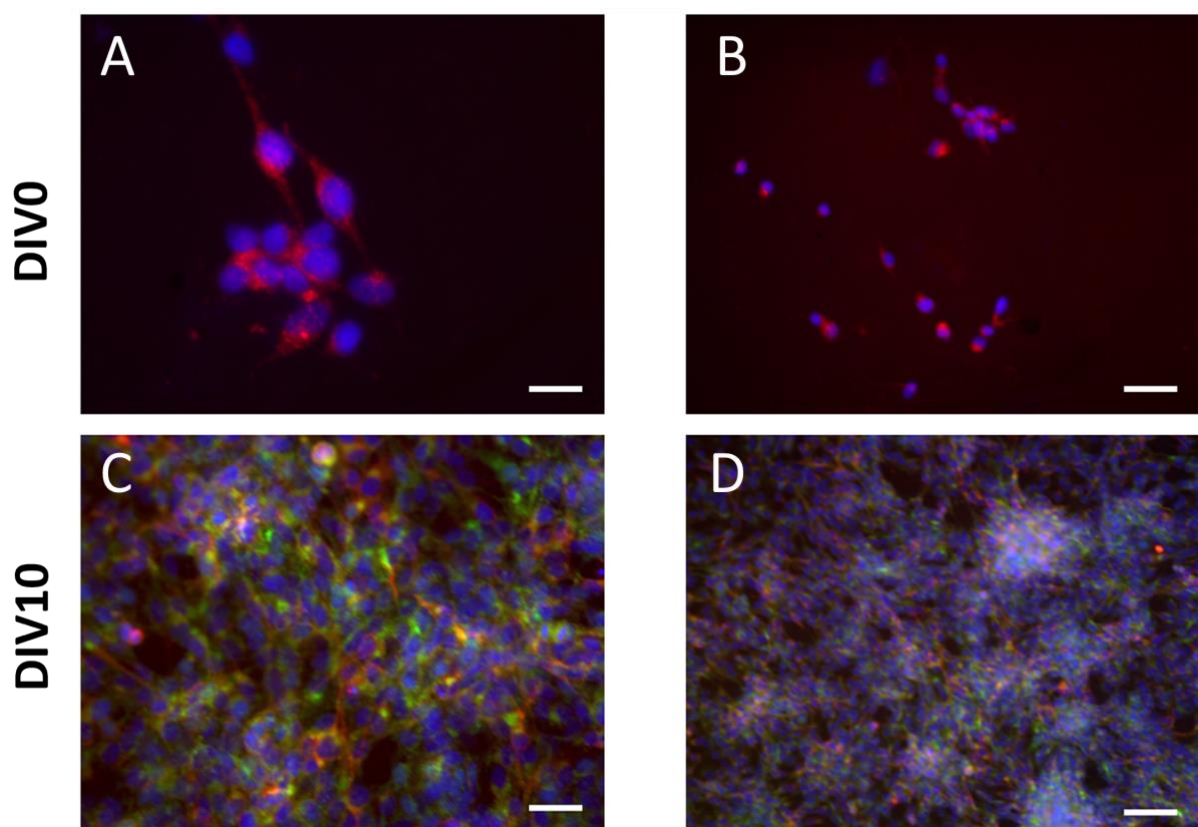


Figure 4. Optical contrast phase images of 2D cell cultures under differentiation labelled for MJFR1 (red, marker for α -synuclein aggregates), MAP2 (green, marker for neuronal cytoskeleton), and DAPI (blue, nuclei). **(A)** SH-SY5Y cells at DIV 0, **(B)** 3K-SNCA cells at DIV 0; **(C)** SH-SY5Y cells at DIV 10, **(D)** 3K-SNCA cells. *Scale bar:* (A) 50 μm , (B-C) 100 μm , (D) 500 μm .

In contrast, **Figure 4C and 4D** clearly show high expression of MAP2, which serves as an indicator of neuronal differentiation. Therefore, we can conclude that the differentiation protocol adapted for both the types of cells promotes differentiation into neuron-like cells.

For the preliminary biocompatibility tests with pH-sensors, SH-SY5Y cells were observed at 4h and 48h after the exposition to pH-sensors. Images were taken in green and red fluorescence and transmission channels. The overlay of the three channels is showed in **Figure 5A** and **5B**, clearly evidencing good biocompatibility without affecting cell proliferation. Furthermore, it was evident that the colour change in the microsensors corresponded to changes in pH values.

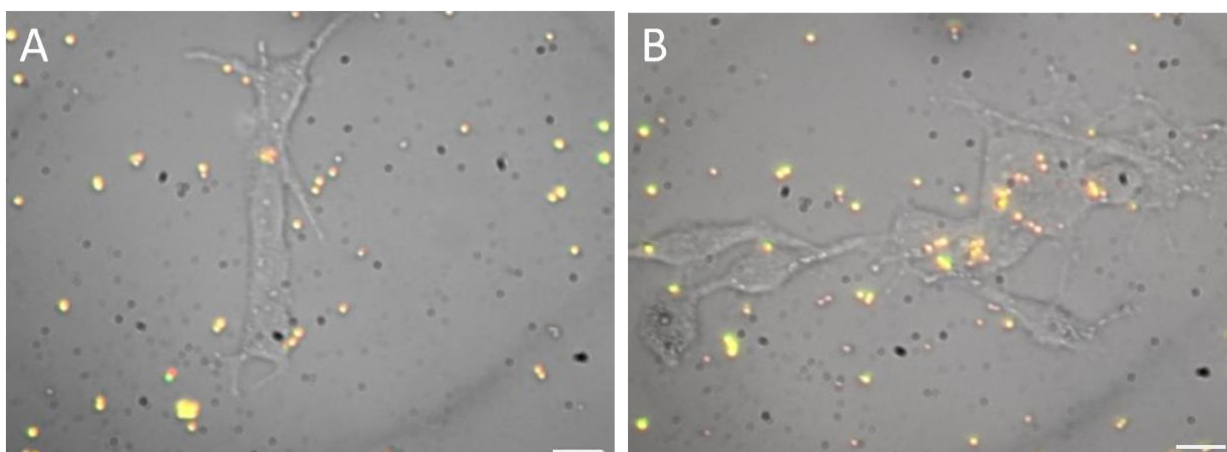


Figure 5. Optical images showing sensors added to SH-SY5Y cell cultures after 4h (A) and 48h (B). Scale bar: 10 μ m.

Subtask 1.3 - Development and characterization of 3D *in vitro* human PD model

This subtask will involve three different activities:

1. Optimized 2D differentiation method for iPSCs PD mutation screening
 - a. Electrophysiology of 2D PD model (12 months)
2. Optimization of 3D model (bioink, hydrogel) (6 months)
3. Optimized 3D differentiation method for iPSCs PD mutation screening
 - a. Electrophysiology of 3D PD model (24 months)

Subtask 1.4 - Application of sensors to 3D human PD model

This subtask will involve two different activities:

1. Application of the pH-sensors on 2D cultures for expansion of investigation on lysosomal physiology
 - a. Electrophysiology of 2D PD model (12 months)
 - b. Drug screening (6 months)
2. Application of the pH-sensors on 3D cultures for expansion of investigation on lysosomal physiology
 - a. Electrophysiology of 3D PD model (12 months)
 - b. Drug screening (6 months)

Subtask 1.5 - Estimation of the acidification time in single living cells over time and space

This subtask will be focused on the application of fully automated computational approaches for measuring acidification in the PD *in vitro* models. Measured pH will be correlated to the electrophysiological activity recorded by microelectrode arrays obtained in Subtask 1.4 and to the effect of pharmacological treatments (20 months).

3 DISSEMINATION ACTIVITIES (SCIENTIFIC PAPERS, POP MAGAZINES, TV, ETC.)

- 30.09.2022. European Researchers' Night 2023, Monastero degli Olivetani, Lecce, Italy. Federica Carnevali, Francesco Colella, Eliana D'Amone, Stefania Forciniti, Giuliana Grasso, Helena Luele, Valentina Onesto, Ilaria Serra,

Anna Chiara Siciliano, Loretta L. del Mercato. Optical sensors and multifunctional biomaterials for applications in precision medicine and biorobotics (poster).

- 18.09.23-21.09.2023. European Materials Research Society (EMRS) Fall Meeting, Warsaw, Poland. Grasso Giuliana, Onesto Valentina, Silvestri Niccolò, Camargo de Oliveira Carolina, Pellegrino Teresa, Loretta L. del Mercato. Multifunctional stimuli-responsive bioengineered systems for cancer therapy: towards precision medicines. Session IO1 – symposium I: Synthesis and characterization of functional nanocomposite materials (oral presentation).
- 18.09.23-21.09.2023. European Materials Research Society (EMRS) Fall Meeting, Warsaw, Poland. Helena Luele, Onesto Valentina, Forciniti Stefania, Colella Francesco, Loretta L. del Mercato. Design and Application of pH-sensing Hybrid systems for noninvasive metabolism monitoring in 3D tumour models. Session IO2 – symposium I: Synthesis and characterization of functional nanocomposite materials (oral presentation).
- 10-13.09.2023. EUROSENSORS, XXXV Conference, Lecce, Italy. Anna Chiara Siciliano, Stefania Forciniti, Valentina Onesto, Helena Luele, Giuseppe Gigli, Loretta L. del Mercato. 4D Optical Mapping of pH in 3D Cell Systems (oral presentation).
- 04-08.09.2023. 33rd Annual Conference of the European Society for Biomaterials (ESB 2023), Davos, Switzerland. Stefania Forciniti, Valentina Onesto, Niccolò Silvestri, Sabrina Hochheim, Carolina Camargo de Oliveira, Teresa Pellegrino, Loretta del Mercato. Biomimetic platforms for in vitro cell growth and biomedical applications: towards precision medicine. Session S7.2: SSB+RM meets ESB: Programmable Biomaterials (oral presentation).
- 04-08.09.2023. 33rd Annual Conference of the European Society for Biomaterials (ESB 2023), Davos, Switzerland. Onesto Valentina, Stefania Forciniti, Helena Luele, Francesco Colella, Daniele De Martino, Loretta L. del Mercato. Hybrid pH-sensing systems for precisely probing single-cell acidification in in vitro tumor models. Session S2.2: Sensing cells and their microenvironments (oral presentation).
- 04-08.09.2023. 24th Conference on Material Science (YUCOMAT 2023 - MRS Serbia), Herceg Novi-Montenegro. Francesco Colella, Valentina Onesto, Giuliana Grasso, Stefania Forciniti, Loretta L. del Mercato. Design and synthesis of a fluorescent ratiometric microsensor for potassium cations tracking (oral presentation).
- 27.05.23-02.06.2023. European Materials Research Society (EMRS) Spring Meeting, Strasbourg, France. Onesto Valentina, Stefania Forciniti, Helena Luele, Francesco Colella, Daniele De Martino, Loretta L. del Mercato. Smart functional pH-sensing scaffolds for extracellular pH mapping in in vitro tumor models. Session H04 – symposium H: Advanced strategies for smart functional and multifunctional biomaterials and biointerfaces (oral presentation).
- 27.05.23-02.06.2023. European Materials Research Society (EMRS) Spring Meeting, Strasbourg, France. Stefania Forciniti, Valentina Onesto, Francesca Serio, Niccolò Silvestri, Carolina Camargo de Oliveira, Teresa Pellegrino, Loretta del Mercato. Stimuli-responsive platforms for in vitro cell growth and cancer therapy: towards precision medicine. Session JO6 – symposium J: Design and scaling up of theranostic nanoplatforams for health: towards translational studies (oral presentation).

Scientific Papers

- Multilayer Polyelectrolyte Capsules for Sensing and Drug Delivery: Fundamentals and Applications. L. L. del Mercato, S. Leporatti, M. M. Ferraro, N. A. Hanafy, R. Rinaldi, W.J.Parak and S. Carregal-Romero. In "Bio-Nano Interfaces". Chapter 57. Pag. 1385-1429. Ed. Wolfgang J. Parak, Jenny Stanford Publishing, www.jennystanford.com, in Press 2024.
- Fluorescent nano- and microparticles for sensing cellular microenvironment: past, present and future applications (2023) Grasso G., Colella F., Forciniti S., Onesto V., Luele H., Siciliano A.C., Carnevali F., Chandra A., Gigli G., del Mercato L.L. *Nanoscale Advances* 2023, 2023,5, 4311-4336. Front cover.
- pH-Sensing Hybrid Hydrogels for Non-Invasive Metabolism Monitoring in Tumor Spheroids (2023) Rizzo R., Onesto V., Morello G., Luele H., Scalera F., S. Forciniti, Gigli G., Polini A., Gervaso F., del Mercato L.L. *Materials Today Bio*, 2023, 20, 100655.

4 MEETINGS IN THIS PERIOD

- February 28 2023: Andolfi (UNIGE), Del Mercato (CNR), Di Lisa (Unige), Pastorino (UNIGE) via TEAMS
- May 30 2023: Andolfi (UNIGE), Di Lisa (Unige), Luele (CNR) via TEAMS

- August 7 2023: Di Lisa (UNIGE), Onesto (CNR) via TEAMS
- September 3 2023: Di Lisa (UNIGE), Onesto (CNR) via telephone
- September 11 2023: Di Lisa (UNIGE), Onesto (CNR) via TEAMS
- September 16 2023: Di Lisa (Unige), Onesto (CNR) via TEAMS
- September 21-23 2023: Del Mercato (CNR), Di Lisa (Unige), luele Helena (CNR), Onesto (CNR), Pastorino (UNIGE), Chiappalone (UNIGE), Meeting of Activity 10 – Biohybrid Interfaces and Biomaterials (Mission3), CNR Nanotec, Lecce (Le)
- October 3 2023: Di Lisa (UNIGE), Onesto (CNR) via telephone
- October 7 2023: Di Lisa (UNIGE), Onesto (CNR) via telephone

5 RECRUITMENT IN THIS PERIOD

- November 01, 2023, Valentina Pavanati, Female, PhD student, enrolled for 36 months.

REFERENCES

- [1] M. E. Gegg and A. H. Schapira, 'Lysosomal-endolysosomal dysfunction and neurodegenerative diseases', *Neurobiology of Disease*, 2022.
- [2] A. D. Klein and J. R. Mazzulli, 'Is Parkinson's disease a lysosomal disorder?', 2018.
- [3] L. Pla, B. Lozano-Torres, R. Martínez-Máñez, F. Sancenón, and J. V. Ros-Lis, 'Overview of the evolution of silica-based chromo-fluorogenic nanosensors', *Sensors*, vol. 19, no. 23, p. 5138, 2019.
- [4] C. F. Hunt, W. H. Lin, and N. Voulvoulis, 'Evaluating alternatives to plastic microbeads in cosmetics', *Nature Sustainability*, vol. 4, no. 4, pp. 366–372, 2021.
- [5] W. Stöber, A. Fink, and E. Bohn, 'Controlled growth of monodisperse silica spheres in the micron size range', *Journal of colloid and interface science*, vol. 26, no. 1, pp. 62–69, 1968.
- [6] B. H. Falkenburger, T. Saridaki, and E. Dinter, 'Cellular models for Parkinson's disease', *Journal of neurochemistry*, vol. 139, pp. 121–130, 2016.
- [7] S. Cetin, D. Knez, S. Gobec, J. Kos, and A. Pišlar, 'Cell models for Alzheimer's and Parkinson's disease: At the interface of biology and drug discovery', *Biomedicine & Pharmacotherapy*, vol. 149, p. 112924, 2022.
- [8] J. L. Biedler, S. Roffler-Tarlov, M. Schachner, and L. S. Freedman, 'Multiple neurotransmitter synthesis by human neuroblastoma cell lines and clones', *Cancer research*, vol. 38, no. 11_Part_1, pp. 3751–3757, 1978.
- [9] S. P. Presgraves, T. Ahmed, S. Borwege, and J. N. Joyce, 'Terminally differentiated SH-SY5Y cells provide a model system for studying neuroprotective effects of dopamine agonists', *Neurotoxicity research*, vol. 5, pp. 579–598, 2003.

Piano Nazionale Complementare (PNC) – Decreto Direttoriale n. 931 del 6 giugno 2022 – Avviso per la concessione di finanziamenti destinati ad iniziative di ricerca per tecnologie e percorsi innovativi in ambito sanitario e assistenziale

Project identifier: PNC0000007

Start date: 01/12/2022

Duration: 44 months

Website: www.fit4medrob.it

ACTIVITY 10– BIOHYBRID INTERFACES AND BIOMATERIALS

SUBACTIVITY#2

RESEARCH TEAMS PERIODIC REPORT, M1-M12

PIs: Luigi Carbone (CNR), Emma Chiaramello (CNR)
Partner Acronym: CNR NANOTEC, CNR IEIIT, UniGenova, UniSalento
Date: 16/10/2023

TABLE OF CONTENTS

1 Deliverables worked on during this period 3

2 Subactivity#2: functional nanoparticles for biorobotics and rehabilitation..... 3

 2.1 Achievements..... 8

3 Dissemination activities (scientific papers, pop magazines, tv, etc.) 12

4 Meetings in this period..... 12

List of abbreviations 12

References 13

1 DELIVERABLES WORKED ON DURING THIS PERIOD

- D 10.1 – Subactivity#2: *Functional nanoparticles for biorobotics and rehabilitation*

2 SUBACTIVITY#2: FUNCTIONAL NANOPARTICLES FOR BIOROBOTICS AND REHABILITATION

Below is a detailed description of the sub-activity, the aim, the breakdown into subtasks, and their time development.

AIM: Due to their unique optoelectronic, magnetic, electric, (photo)-catalytic, and chemical properties stemming from nanoscale confinement, colloidal inorganic nanoparticles have encountered wide popularity in biomedical fields as possible agents for imaging, theranostic, or drug delivery purposes.[1-3] Also, the thorough knowledge gained in the synthesis procedures of colloidal nanoparticles has allowed researchers to design complex breed-new multicomponent nanoarchitectures built upon the creation of heterointerfaces amongst different materials.[4] In this view, distinct domains can be accurately organized into core-shell or hetero-oligomer topologies through the formation of epitaxial heterojunctions. Wet-chemical synthetic strategies have indubitably proved effective in heterostructure engineering as well as in the control of the final geometries, crystal habit, and surface functionalities.[5, 6]

A new brand of colloidal inorganic nanoparticles under strict monitoring because of interesting potential in nanomedicine, spintronics, and electrocatalysis are multiferroic MENPs.[1, 6, 7] Owing to the existence of the ME effect, an intrinsic coupling between magnetic and electric fields occurs in these materials. Generally, such heterostructured materials consist of a magnetostrictive domain which converts a magnetic field into a vibrational lattice strain, and a piezoelectric domain which converts the strain generated at the heterointerface (the coupling area) into an electric field. This electric field induces also the formation of charge carriers. High values of ME voltage coefficients express the efficiency of energy conversion from magnetic field to electricity.

The possibility of eliciting high amplitude electric fields when stimulated wirelessly by small amplitude magnetic fields opens a wide range of applications in the biomedical domain, and in particular for the modulation of the nervous system activity. Some proof of concepts towards the use of MENPs as nanoelectrodes for wireless central nervous stimulation were described, both in computational studies[8, 9], and in experimental approaches, e.g., in vitro[10], ex vivo[11], or in vivo studies[12, 13]. All these approaches confirmed the feasibility of using MENPs for obtaining single-neuron spatial resolution coupled with minimal energy dissipation and remote activation and control through a safe magnetic source.

These characteristics could play a crucial role in the modulation and stimulation of the peripheral nervous system, in particular considering the increasing interest in new stimulation techniques, less invasive but with higher selectivity that had a rapid development in prosthetic technologies to achieve sensory feedback control with desirable high spatial and temporal resolution.

The sub-activity ‘Functional nanoparticles for biorobotics and rehabilitation’ aims at realizing active nanomaterials for the stimulation of the peripheral nervous system with applications in the field of neurorehabilitation (Figure 1). ME heterostructured colloidal nanoparticles, i.e. nanosized core-shell magneto-electric materials, will be engineered and suitably incorporated within biocompatible hybrid scaffolds, for the selective stimulation of nerve fibres at the interface with prosthetic systems. The as-developed hybrid materials will be characterized through in silico approaches and in vitro experiments; the development and handling of such materials will offer the possibility of overcoming the limitations of current peripheral nerve stimulation techniques, offering a completely new and versatile tool in terms of spatial and temporal resolution and controllability of interface phenomena opening new possibilities for prosthetic technologies.

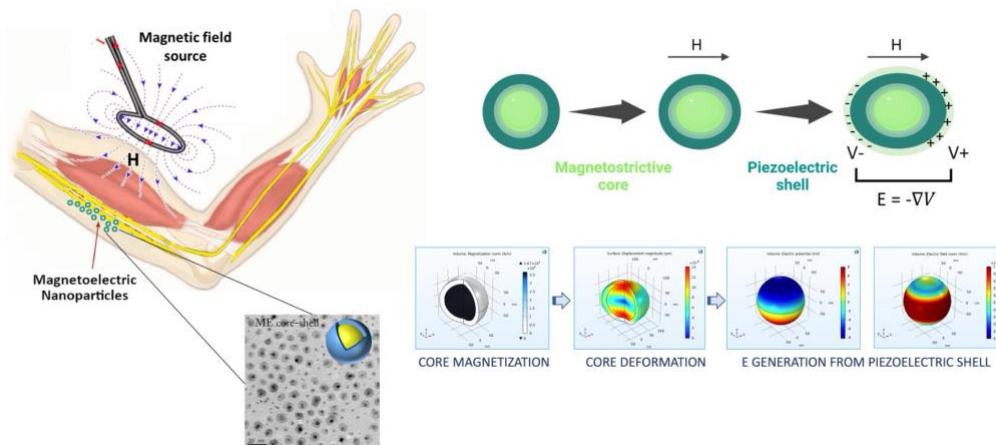


Figure 1. Graphical abstract of SubActivity#2.

WORKPLAN

Figure 2 below summarizes the sub-activity architecture organized according to eight different subtasks distributed amongst experimental works and numerical simulations. Figure 2 highlights in yellow the presence of Subtask 2.9 concerning in vivo testing of MENPs and MENPs/scaffold hybrid material. The subtask is currently under development and elaboration; this activity would be carried out depending on findings of the previous subtasks and on realization constraints that could arise during the sub-activity progress. Of course, this subtask will involve a related activity of computational modeling. More details will be provided in the coming months with the definition of activities and objectives for this subtask. The sub-activity timeline relative to each subtask is reported in Figure 3 in the Gantt chart. Hereafter, each subtask is shortly described.

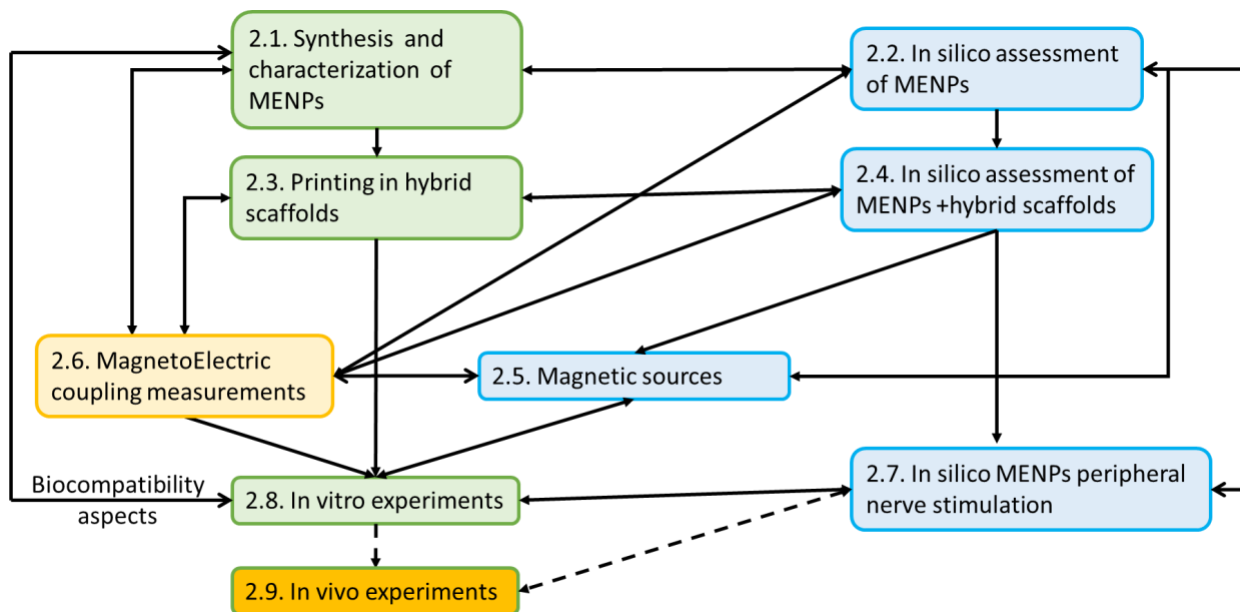


Figure 2. Subactivity 2 Pert Chart

measurements will also provide information regarding the wettability of these scaffolds, crucial information when considering the influence of biomaterial properties on cell adhesion and cell growth.

Subtask 2.4 - In silico assessment of MENPs in hybrid scaffolds.

Starting from knowledge of the ME effects at the nanoscale around a single MENP learnt from **Subtask 2.2**, **Subtask 2.4 has the goal of developing in silico models of the ME behaviour of MENPs when placed in hybrid scaffolds with different mechanical and dielectric properties, considering the influence of the reciprocal positions and concentrations of MENPs, and all the other features that could be experimentally controlled.**

Similarly to Subtask 2.2, the methodology applied will be computational approaches based on multiphysics, able to consider all the physical aspects involved in the ME phenomenon.

The expected results will be the in silico evaluation of the electric field elicited by different concentrations of MENPs, placed in hybrid scaffolds, to identify the best MENPs-scaffold arrangement for peripheral nerve stimulations. Results from this activity will provide the information needed for printing of MENPs in hybrid scaffolds (Subtask 2.3) and for the “In silico MENPs peripheral nerve stimulation” (Subtask 2.7).

Subtask 2.5 - Magnetic sources.

Starting from knowledge of the ME effects learnt from Subtask 2.2 and Subtask 2.4, **Subtask 2.5 has the main objectives to (1) in-silico design and characterize magnetic sources in terms of DC field magnitude, AC field magnitude, AC field frequency, and uniformity of the magnetic fields (H) needed for in vitro experiments; (2) design and manufacture the magnetic source for in vitro experiments.** The system will be designed using computational electromagnetics techniques. **The expected results will be the design, manufacture, characterization, and validation of the magnetic source for the in vitro experiments performed in Subtask 2.8.** In case Subtask 2.9-“In vivo experiments” will be carried out, Subtask 2.5 will take care also of the magnetic source development for this experimental phase.

Subtask 2.6 - MagnetoElectric coupling measurements.

ME effects are observed in multiferroic solids that simultaneously possess both the ferromagnetic and ferroelectric ordering. ME coupling is described by the ME coefficient (α_{ME}), which results from the mechanical interfacial coupling between the magnetostrictive core and piezoelectric shell and can be expressed as:

$$\alpha_H = \left(\frac{\partial P}{\partial H} \right) \quad (1)$$

and

$$\alpha_E = \left(\frac{\delta M}{\delta E} \right) \quad (2)$$

describing, respectively, the change in the electric polarization P due to the application of a magnetic field H (direct effect) or the change in the magnetization M of a substance under the action of an electric field E (converse effect).[23]

The magnetically-induced (α_H) and electrically-induced (α_E) ME coefficients are thermodynamically equivalent.[23]

By examining α_H and considering the dielectric permittivity of the vacuum (ϵ_0) and the relative permittivity of the medium (ϵ_r), and assuming $\epsilon_r \gg 1$ (for materials with dielectric constant much larger than 1), equation (1) can be rewritten as:

$$\alpha_H = \left(\frac{\partial P}{\partial H} \right) \cong \epsilon_0 \epsilon_r \left(\frac{\partial E}{\partial H} \right) = \epsilon_0 \epsilon_r \frac{1}{t} \left(\frac{\partial V}{\partial H} \right) = \epsilon_0 \epsilon_r \alpha_H^V \quad (3)$$

where α_H^V represents the magnetically-induced voltage ME coefficient and t the thickness of the dielectric material. **As it is easier to determine a voltage than an electric polarization, the measurement of the α_H^V is preferred and commonly associated with the general description of the ME coefficient α_{ME} .**

$$\alpha_H^V = \alpha_{ME} = p \times \lambda = \left(\frac{\partial E}{\partial H} \right) = \frac{1}{t} \frac{\Delta V}{\Delta H} \left(\frac{1}{cm \cdot Oe} \right) \quad (4)$$

where p and λ are piezoelectric and magnetostrictive coefficients, respectively.[7, 23]

To provide reliable data of the ME coupling of MENPs, the determination of α_{ME} is crucial. **Generally, the exact values of the ME voltage coefficient can be obtained by measuring the output voltage signals induced by the MENPs under an applied magnetic field.** ME measurements are conducted under a dynamic AC magnetic field (H_{AC}) superimposed with a DC magnetic field bias (H_{DC}), while measuring the electrical voltage response using a lock-in amplifier. While a ME response can be obtained with just an H_{AC} , large AC fields are required to approach the maximum α_{ME} , which would require powerful coil systems and additional components to enable active cooling; nevertheless, the literature has demonstrated that large H_{DC} obtained using permanent magnets overlaid on a smaller H_{AC} can maximize α_{ME} . [13] **ME coefficients can be determined through either bulk specimen-based measurements of magnetically-induced ME coupling or single NP-based techniques.** In the former case, ME composite is easily prepared by incorporating MENPs within a polymer matrix; usually, bulk sample measurements provide reduced values of the polarization of the

piezoelectric material, meaning that it is difficult to fully polarize the piezoelectric phase, because of possible charge leakage caused by the conductive polymer. This method, however, does not allow for determining the exact α_{ME} of a single MENP due to size deviation and/or NP aggregates.[7] To avoid such effects the optimum is to measure α_{ME} at the nanoscale, although its determination at single NP level is highly challenging. This can be achieved via Scanning Probe Microscopy techniques such as MFM, PFM, and EFM.

Bulk specimen-based approaches for the determination of the ME coefficient of MENPs originating from the research lines of subtask 2.1 will be performed through collaboration with the Omnic Research Group (<http://www.omnics.it/home/>), an interdisciplinary research team of University of Salento whose activities are carried out in laboratories located at the Characterization Facility of CNR NANOTEC, that boast expertise in the electronics, spintronics and magnonics fields. Single NP-level ME coefficient measurements will be performed at CNR NANOTEC through PFM analysis under ($H_{DC} + \delta H_{AC}$) magnetic stimulation.

Subtask 2.7 - In silico MENPs peripheral nerve stimulation.

Starting from knowledge of the ME effects learnt from subtask 2.2 and subtask 2.4, **subtask 2.7 has the main goal of characterizing the electromagnetic interaction between MENPs printed in hybrid scaffolds and peripheral nerves, by accounting for the most realistic reciprocal positioning and influence of the surrounding tissues and materials.** The main methodologies used will be computational electromagnetic approaches coupled with models of neuronal dynamics. The expected results will be the in-silico evaluation of the interaction between the most promising MENPs-hybrid scaffold combinations and realistic peripheral nerves, to identify the most promising reciprocal localization between MENPs and nerves, and to assess the spatial resolution and efficacy of the stimulation. The results of this Task will allow for obtaining information needed for identifying the best experimental conditions for the experiments expected in subtask 2.8, and eventually in subtask 2.9.

Subtask 2.8 - In vitro experiments.

The first activity of this subtask is aimed at assessing the biocompatibility of the MENPs in neuronal cell models. The surface of the as-synthesized MENPs will be coated by hydrophilic/amphiphilic molecules, as already reported, to afford their solubility and colloidal stability in aqueous and biological media. **The biocompatibility and proliferation of immortalized neuronal cells upon incubation with the MENPs will be evaluated by conventional colorimetric and fluorometric assays.** The nanoparticles with the best biocompatibility profile will be then used for further cellular studies. **Immortalized neuronal cells will be administered with the nanoparticles and their response upon application of an external magnetic stimulus will be evaluated.** The morphology and the elongation of the cells will be studied upon variation of the incubation conditions (MENPs concentration, incubation time, and magnetic field intensity), as well as the expression of specific neuron-specific proteins.

Furthermore, the interplay between neuronal cells and MENPs-loaded scaffolds will be investigated. To this aim, the capability of the neuronal cells to adhere to, proliferate on the scaffold surface, and “sense” the ME stimulation will be evaluated. In this condition, it will be critical to investigate whether the distance between MENPs and cells and the spatial distribution of the nanoparticles into the scaffold provide a physical barrier to the ME stimulation of the cell membrane.

Tests of extracellular stimulation and recording of the in vitro electrophysiological activity on 2D and 3D neuronal models based on (2D and/or 3D) multielectrode arrays will also be performed, through collaboration with the bioengineering group by UniGenova.[24] Peripheral nerve function, network communication, and response to ME output occurring via MENP-assisted magnetic-to-electric field generation will be evaluated.

Subtask 2.9 - In vivo experiments

During the workshop of 22 September 2023 held at the Lecce site of CNR NANOTEC, the possibility of including in the architecture of sub-activity 2 an in vivo experimental activity based on MENPs and MENPs/scaffold hybrid materials, respectively, emerged. Application hypotheses concerning examples of in vivo (or ex vivo) models were put forward by Prof. Carmelo Chisari and Dr. Stefania Dalise (Azienda Ospedaliero-Universitaria Pisana), and the possibility of acquiring in vivo models for computational simulation was also evaluated. Some examples of in vivo experimentation already reported in the literature based on the use of MENPs corroborate the hypotheses and confirm the feasibility of the experiments, as well as the urgency of experimental and in silico validation.[13, 25] The subtask 2.9, is highlighted in yellow to point its provisional condition out; the Task is currently being studied and elaborated. From a time perspective, at present, we assume the start of this activity around project month 30 (May 2025), as indicated in Figure 2. Definitive details will be provided in the next report.

2.1 ACHIEVEMENTS

The sub-activity started its research activity in February 2023, with Subtask 2.2, which concluded its activities in August 2023. In September 2023 Subtask 2.1, 2.4, and 2.7 started their activities, also. A description of the ongoing activities and achievements is reported below.

Subtask 2.1

This subtask describes preparative methodologies developed by CNR NANOTEC for the liquid-phase chemical synthesis of MENPs with controlled structural (crystalline phase), geometrical (size, morphology), and surface (protective "capping" molecules) characteristics that can be precisely correlated with experimental process parameters (temperature, concentration and relative ratio of reagents, synthesis technique). **The report describes in detail the first examples of synthetic protocols reproduced from the literature for the preparation, extraction, and purification of NPs of Fe_3O_4 and $\text{Co}_x\text{Fe}_{3-x}\text{O}_4$ with isotropic geometries.** The procedures described refer to experiments conducted on the typical scale of a research chemical laboratory, equipped with state-of-the-art equipment, or using a setup as shown in the sketch on the left in Figure 3.

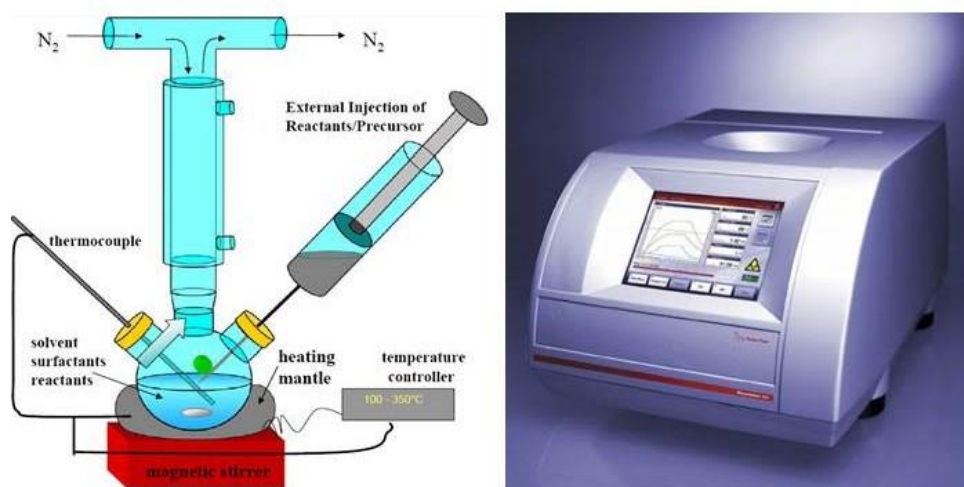


Figure 4. The left image shows a schematic of the experimental apparatus generally employed for the synthesis of colloidal nanocrystals. The picture on the right side displays a microwave reactor Anton Paar Monowave 300 used for μW -assisted synthesis (<https://www.anton-paar.com/corp-en/products/details/microwavesynthesis-monowave-400200/>). This equipment allows the measurement of the pressure developed during the synthetic step and temperature. The latter is determined by simultaneously employing an infrared probe and a Rubidium thermocouple directly immersed in the reaction mixture.

The syntheses are conducted, at atmospheric pressure, in three-neck glass flasks (50-500 mL) connected to a vacuum/Nitrogen Schlenk line, heated through electric mantles, and equipped with internal probes for temperature control and mechanical or magnetic stirrers to allow mixing of the reaction liquid. Where necessary, the handling of reagents (in particular, organometallics) is conducted in a glove-box under an inert atmosphere of Nitrogen. Further experiments were conducted using a μW reactor as the heating methodology (see right picture of Figure 4). The use of microwaves makes it possible to i) work in hermetically sealed environments from the outside, so overpressure conditions are often created that are useful for synthetic purposes, particularly when working in an aqueous environment; ii) selectively heat only those reactants that can absorb microwaves; and iii) place multiple syntheses simultaneously in a single reaction rack. However, despite these operational differences from the conventional heating method, the literature has amply demonstrated that unexpected thermal effects do not occur compared to the classical convective flows of the conventional method.

The activities of this subtask that began a few weeks ago have so far focused on the synthesis of magnetic NPs via thermal decomposition in an organic ambience (solvothermal) either occurring via μW approaches or in a reaction flask (Schlenk line). Following examples from the literature we focused on the growth of spherical NPs of Fe_3O_4 and $\text{Co}_x\text{Fe}_{3-x}\text{O}_4$, the latter according to different Co-to-Fe stoichiometric ratios, showing the following features: i) surface

capping made by OLAC, OLAM, and/or 1,2-hexadecanediol; ii) solubility in low to medium viscosity nonpolar solvents; iii) appreciable degree of size monodispersion; iv) absence of aggregation phenomena; v) dot-like morphology. The protocol exploits thermal decomposition reaction occurring in non-coordinating or weakly coordinating organic solvents such as ODE or phenyl ether, whereas OLAC and OLAM contribute to complexing the metal ions (Fe and Co) thus moderating their reactivity and stabilizing the final NP by passivating the surface.

Microwave-assisted synthesis of Fe_3O_4 and $\text{Co}_x\text{Fe}_{3-x}\text{O}_4$. $\text{Fe}(\text{acac})_3$ (1 mmol) is mixed with 4 ml of OLAC, 10 ml of OLAM, and 2 ml of ODE in a 30 ml Pyrex vessel suitable for microwave irradiation (see Figure 3, right picture). The batch is slowly heated at 200°C (in 10 min starting from room temperature) and the temperature is kept for 10 min. Afterward, the temperature is raised to 250°C (in 15 min) and the sample is heated for a further 5 min; after this time, the system is cooled through a Nitrogen flow. The NPs are then washed by precipitation with a mixture of ethanol and acetone and resuspended in hexane; this procedure is repeated twice to purify the sample from non-reacted reagents.[26] Superparamagnetic NPs (5-10nm) are expected although magnetic characterization has not been performed yet.

A similar protocol has been employed for the growth of $\text{Co}_x\text{Fe}_{3-x}\text{O}_4$ NPs; in this case, $\text{Co}(\text{acac})_2$ has been added to the reaction mixture above described to realize the following Co-to-Fe stoichiometric ratios, 1:2, 0.8:2.2, and 0.6:2.4, in all cases keeping the total amount of metal ions (Co+Fe) constant to 1 mmol. In all the described examples of both Fe_3O_4 and $\text{Co}_x\text{Fe}_{3-x}\text{O}_4$, spherical NPs have been obtained.

Solvothermal synthesis of Fe_3O_4 and $\text{Co}_x\text{Fe}_{3-x}\text{O}_4$ in a Schlenk line (left cartoon in Figure 4). $\text{Fe}(\text{acac})_3$ (2 mmol) is mixed with 10 mmol of 1,2-hexadecanediol, 6 mmol of OLAC, 6 mmol of OLAM, and 20 ml of phenyl ether and stirred under an inert atmosphere (N_2). The mixture is heated to 200°C for 30 min and then the temperature is increased to 265°C for a further 30 min. Then the heating mantle is removed and the temperature let to decrease to room temperature. The synthesis product is purified by precipitation with ethanol under centrifugation and dissolution of the collected black precipitate in hexane.[27, 28] The purification procedure is repeated twice. For the growth of $\text{Co}_x\text{Fe}_{3-x}\text{O}_4$, $\text{Co}(\text{acac})_2$ is added to the reaction mixture in the desired molecular ratios keeping the total concentration of metal ions constant.

Morphological, structural, compositional, and magnetic characterization tests/analyses are in progress. Additionally, in the next weeks, hydrothermal syntheses of Fe_3O_4 and $\text{Co}_x\text{Fe}_{3-x}\text{O}_4$ will be investigated.

Subtask 2.2

The in silico assessment was based on the most widely used configuration of MENPs, i.e. the core-shell system based on CoFe_2O_4 (Cobalt Ferrite, CFO, spinel structure)— BaTiO_3 (Barium Titanate, BTO, perovskite structure). CFO is a hard magnetic material that shows a ferromagnetic behavior at room temperature, while BTO presents spontaneous electric polarization and piezoelectric properties. Core-shell nanostructures are widely adopted to maximize a good interfacial coupling between the core and the shell and, therefore, to ensure proper mechanical-to-electrical signal transduction.[7, 29] In this regard, tuning the electromagnetic properties by changing the morphology of the MENPs from the traditional spherical particles to other nanostructures (e.g., nanorice, nanorods, nanotubes, nanowires, etc.) opens up enormous possibilities and widens MENPs applications and performances. In this framework, in silico investigations are of paramount importance to define the MENPs' operational range for a specific bio-application.

Considering the above-mentioned premises, in this subtask, the magnetoelectrical behavior, in terms of ME coupling coefficient (α_{ME}), of core-shell MENPs with different shapes was analyzed through a numerical model. The nanostructures were initially subjected to a high-amplitude DC magnetic field to assess their electrical output. Moreover, a following study was performed under a time-variant and low amplitude magnetic field at low frequency (50 Hz), as several recent works reported how this type of magnetic stimulation commonly adopted for biomedical applications can yield an improved ME response.[30-35] Results of this study pinpoint the possibility of efficiently modulating the MENPs' electrical output also by varying their geometrical features, an approach less investigated so far.

Figure 4 shows different MENPs morphologies considered in the subtask, i.e., sphere with spherical core (SPH), sphere with cubic core (SPH-C), spindle (SPI), nanocable (NCB), nanorod (NR). SPH, SPI, and NCB geometries presented comparable volumes, while for NR, two main constraints have been considered: a) its morphology implies a strong preferential axis of growth; b) the core volume has to be comparable with those of the other structures since this feature strongly affects the electrical performance.[35] Therefore, the NR dimensions were set to 1) keep rather constant the core volume with respect to the other geometrical configurations, 2) guarantee a strong geometrical anisotropy (>2), and 3) be consistent with NRs fabricated in experimental studies.[36-39]

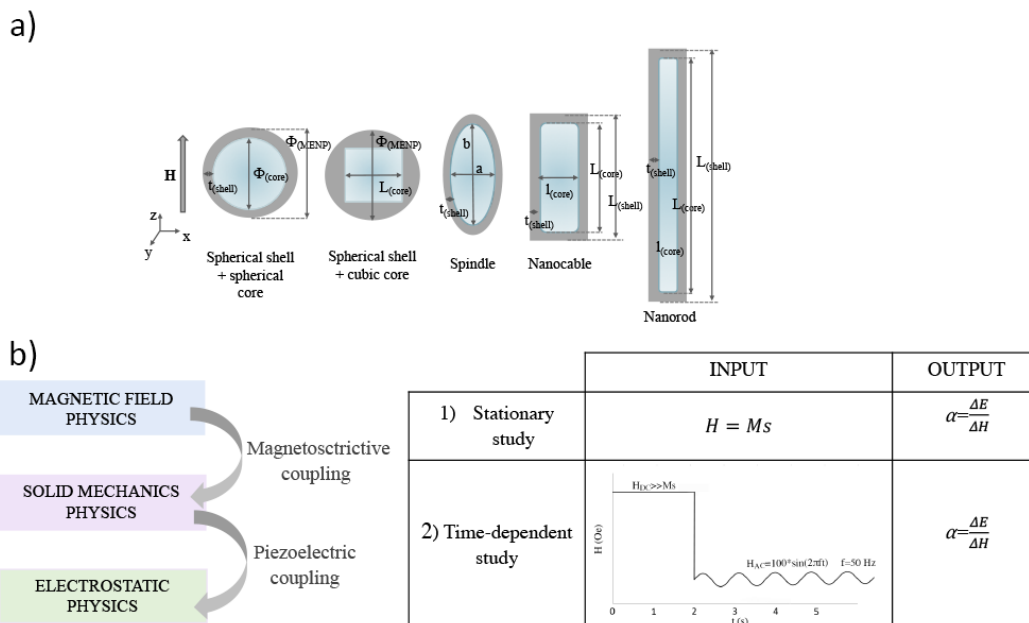


Figure 5. MENPs morphologies and modeling parameters. (A) Sketches representing the different ME nanostructures under study, with the corresponding dimensions. (B) MENPs computational study workflow and simulation settings (taken from Ref.[40]).

As to the magnetic fields eliciting the ME behavior, both stationary studies based on the use of an external uniform magnetic field directed along the z-axis at which amplitude was set to be higher than the magnetic saturation (M_s), and time-dependent analyses with uniform magnetic field directed along the z-axis at extremely low frequency and low amplitude ($f = 50$ Hz, 100 Oe) were considered. In this latter case, the time-varying magnetic field was applied after a DC pre-magnetization step through high amplitude excitation ($\gg M_s$) (see Figure 5). All the computational steps, shown in Figure 4b, were implemented using COMSOL Multiphysics® 5.6 (www.comsol.com). For more details about the computational approach, see Refs [35, 40].

As an example of the obtained results, Figure 6 shows the 3D distribution of electric potential V (mV), on CFO-BTO core-shell nanostructure surfaces, when stimulated with a uniform DC magnetic field at saturation. The electric potential difference generated between the extremities of the nanostructures increases by changing their shape (from the spherical reference to more elongated structures), reaching a maximum value of 20.5 mV for the NR, thus suggesting the most efficient ME behaviour. When considering the corresponding ME coefficient, estimated as the ratio between the maximum electric field intensity derived at the MENP outer border and the change in the external magnetic field, the influence of the different geometries is quite evident, as shown in Figure 7. The amplitude of the ME coefficient remarkably grew as follows ($NR \gg NCB > SPI > SPH$). When considering the area at the interface between the magnetostrictive and piezoelectric phase along with the geometrical anisotropy of the structures under study, results showed that the NCB and NR interfacial areas are comparable and higher than the SPH and SPI systems, while the anisotropy is incremented of 5-folds when passing from the nanosphere to the nanorod. Taken together, these observations suggest that the interplay between the contributions of both the interface coupling and the shape anisotropy is essential to achieve an ameliorated ME response.

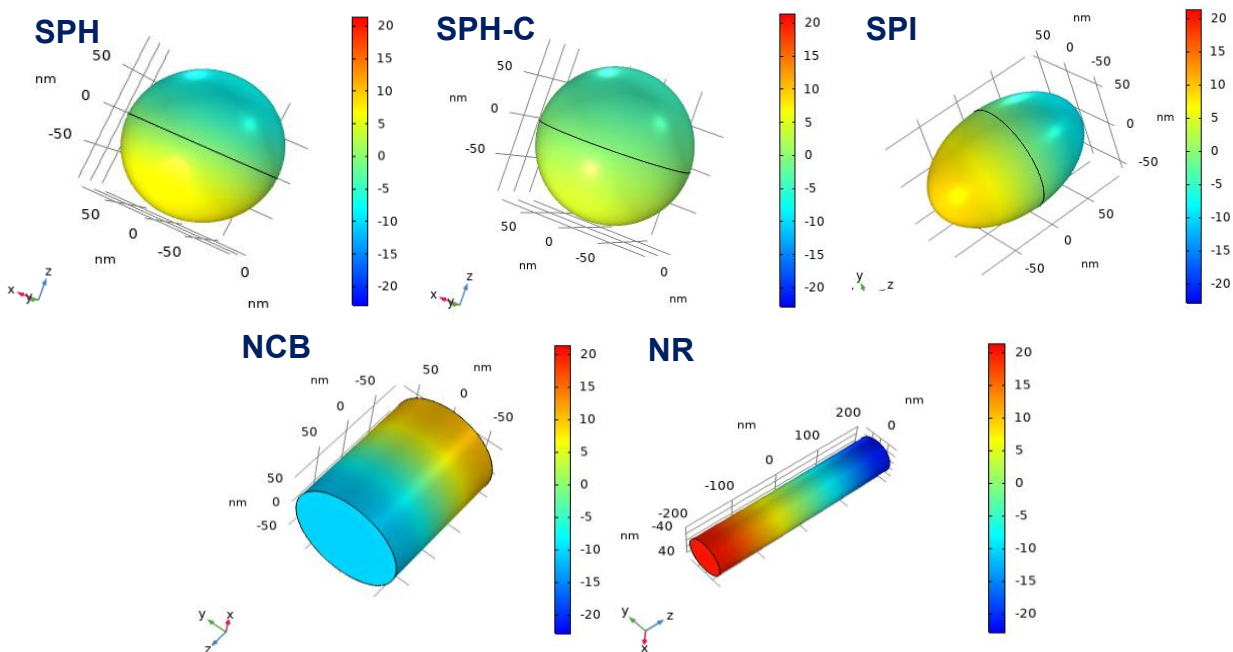


Figure 6. ME effect induced by DC magnetic field stimulation. 3D distribution of electric potential V (mV), of CFO-BTO core-shell nanostructures, when a DC magnetic field at saturation is applied in the study ($H = M_s$, where M_s is the saturation magnetization).[40]

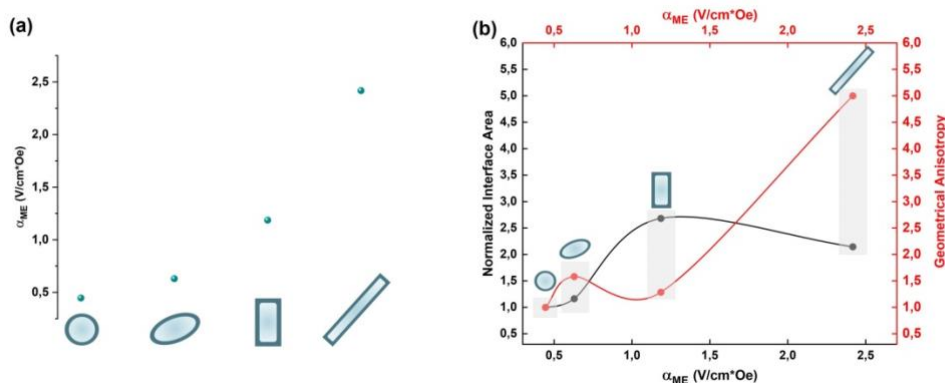


Figure 7. ME nanostructure performances. (A) Effect of the nanostructures geometries on the ME when MENPs are stimulated at saturation ($H = M_s$) in DC conditions. (B) Influence of normalized interface area and geometrical anisotropy on the ME performance. For all the configurations under study, the MENPs are oriented along the direction of the applied external magnetic field H .[40]

In conclusion, results show that MENPs with a more elongated morphology exhibit a superior ME coefficient if compared with spherical nanoparticles of similar volume, for both DC and AC magnetic fields. This response is due to the presence of a larger surface area at the interface between the magnetostrictive core and piezoelectric shell, and to the MENP geometrical orientation along the direction of the magnetic field. Moreover, the locally induced electrical field becomes drastically enhanced under the low amplitude AC field if the material has been pre-magnetized, leveraging on the “memory effect” of the core hysteretic behaviour. The herein presented concept can be broadened to engineer various geometrical interphase configurations, thus gaining fundamental knowledge to support MENPs synthesis.

Subtask 2.4

The Subtask just started its activities, by the identification of the main mechanical and dielectric properties of those polymers that (1) can be processed via the conventional fabrication techniques and (2) can be at the basis of the hybrid scaffold in which ME nanostructures will be printed. By using a multiphysics approach similar to the one reported for Subtask 2.2, preliminary computational simulations have been carried out to assess the feasibility of this approach, and the influence of the number of the ME nanostructures within a unit reference of the model, as well as their positioning within the polymeric matrix.

Subtask 2.7

The Subtask just started its activities. The most promising approach for in silico assessment of the interaction between MENPs printed in hybrid scaffolds and the peripheral nervous system was identified, as well as the most suitable models of neuronal dynamics. Preliminary results were obtained by considering a few MENPs not printed in a hybrid scaffold, but hypothesized to be placed at different positions in the proximity of peripheral nerves, highlighting, as expected, a great influence of the distance between the MENPs and the nerve fibre on the elicited response.

3 DISSEMINATION ACTIVITIES (SCIENTIFIC PAPERS, POP MAGAZINES, TV, ETC.)

The research activities carried on in this first period led to the publication of 1 paper in international peer-reviewed journals and 4 contributions to conference proceedings.

Papers.

- [1] A. Marrella, G. Suarato, S. Fiocchi, E. Chiaramello, M. Bonato, M. Parazzini, & P. Ravazzani, "*Magnetolectric nanoparticles shape modulates their electrical output*", *Frontiers in Bioengineering and Biotechnology*, 2023, 11 <https://doi.org/10.3389/fbioe.2023.1219777>

Conference contributions.

- [2] G. Suarato, A. Marrella, S. Fiocchi, E. Chiaramello, M. Bonato, M. Parazzini, P. Ravazzani, "*Shape effect on the electrical output of magneto-electric nanoparticles*", BioEM 2023, 18 – 23 June 2023, Oxford, UK [3]
- [3] S. Fiocchi, E. Chiaramello, V. Galletta, A. Marrella, G. Suarato, M. Bonato, M. Parazzini, P. Ravazzani, "*A computational framework for magnetolectric nanoparticles application as neural interfaces*", BioEM 2023, 18 – 23 June 2023, Oxford, UK
- [4] V. Galletta, E. Chiaramello, S. Fiocchi, A. Marrella, G. Suarato, M. Bonato, M. Parazzini, P. Ravazzani, "*A new promising approach for motor nerve stimulation: magnetolectric nanoparticles*", BioEM 2023, 18 – 23 June 2023, Oxford, UK
- [5] V. Galletta, E. Chiaramello, S. Fiocchi, A. Marrella, G. Suarato, M. Bonato, M. Parazzini, P. Ravazzani, "*Magnetolectric nanoparticles as promising tools for nerve stimulation*", GNB2023, 21 – 23 June 2023, Padova, Italy

4 MEETINGS IN THIS PERIOD

Meeting CNR NANOTEC-IEIIT, 12.04.2023, Milano. Participants: P. Ravazzani, E. Chiaramello, S. Fiocchi, M. Parazzini, G. Suarato, M. Bonato, A. Marrella, L. Del Mercato, A. Quarta, R. Scarfiello, L. Carbone

LIST OF ABBREVIATIONS

NPs	Nanoparticles
MENPs	MagnetoElectric Nanoparticles
ME	MagnetoElectric
μW	Microwave

SEM	Scanning Electron Microscope/Microscopy
TEM	Transmission Electron Microscope/Microscopy
AC	Alternating Current
DC	Direct Current
MFM	Magnetic Force Microscopy
PFM	Piezoresponse Force Microscopy
EFM	Electric Force Microscopy
CoFe ₂ O ₄	Cobalt Ferrite
CFO	Cobalt Ferrite
BaTiO ₃	Barium Titanate
BTO	Barium Titanate
OLAC	Oleic acid
OLAM	Oleylamine
Fe(acac) ₃	Ferric acetylacetonate
ODE	Octadecene
Fe ₃ O ₄	Iron Oxide Magnetite structure
N ₂	Nitrogen

REFERENCES

- [1] K. Kapat, Q. T. H. Shubhra, M. Zhou, and S. Leeuwenburgh, "Piezoelectric Nano-Biomaterials for Biomedicine and Tissue Regeneration," *Advanced Functional Materials*, vol. 30, p. 1909045, 2020/10/01 2020.
- [2] N. Ashammakhi, A. L. Hernandez, B. D. Unluturk, S. A. Quintero, N. R. de Barros, E. Hoque Apu, *et al.*, "Biodegradable Implantable Sensors: Materials Design, Fabrication, and Applications," *Advanced Functional Materials*, vol. 31, p. 2104149, 2021/12/01 2021.
- [3] E. Hoque Apu, M. Nafiujjaman, S. Sandeep, A. V. Makela, A. Khaleghi, S. Vainio, *et al.*, "Biomedical applications of multifunctional magnetoelectric nanoparticles," *Materials Chemistry Frontiers*, vol. 6, pp. 1368-1390, 2022.
- [4] C. Nobile and P. D. Cozzoli. (2022, Synthetic Approaches to Colloidal Nanocrystal Heterostructures Based on Metal and Metal-Oxide Materials. *Nanomaterials* 12(10).
- [5] P. D. Cozzoli, T. Pellegrino, and L. Manna, "Synthesis, properties and perspectives of hybrid nanocrystal structures," *Chemical Society Reviews*, vol. 35, pp. 1195-1208, 2006.
- [6] P. Wang, E. Zhang, D. Toledo, I. T. Smith, B. Navarrete, N. Furman, *et al.*, "Colossal Magnetoelectric Effect in Core–Shell Magnetoelectric Nanoparticles," *Nano Letters*, vol. 20, pp. 5765-5772, 2020/08/12 2020.
- [7] H. Song, M. A. Listyawan, and J. Ryu. (2022, Core–Shell Magnetoelectric Nanoparticles: Materials, Synthesis, Magnetoelectricity, and Applications. *Actuators* 11(12).
- [8] E. Chiamello, S. Fiocchi, M. Bonato, A. Marrella, G. Suarato, M. Parazzini, *et al.*, "Magnetoelectric Nanoparticles: Evaluating Stimulation Feasibility of the Possible Next Generation Approach for Deep Brain Stimulation," *IEEE Access*, vol. 10, pp. 124884-124893, 2022.
- [9] S. Fiocchi, E. Chiamello, A. Marrella, M. Bonato, M. Parazzini, and P. Ravazzani, "Modelling of magnetoelectric nanoparticles for non-invasive brain stimulation: a computational study," *Journal of Neural Engineering*, vol. 19, p. 056020, 2022/09/23 2022.
- [10] E. Zhang, M. Abdel-Mottaleb, P. Liang, B. Navarrete, Y. A. Yildirim, M. A. Campos, *et al.*, "Magnetic-field-synchronized wireless modulation of neural activity by magnetoelectric nanoparticles," *Brain Stimulation*, vol. 15, pp. 1451-1462, 2022/11/01/ 2022.
- [11] T. Nguyen, J. Gao, P. Wang, A. Nagesetti, P. Andrews, S. Masood, *et al.*, "In Vivo Wireless Brain Stimulation via Non-invasive and Targeted Delivery of Magnetoelectric Nanoparticles," *Neurotherapeutics*, vol. 18, pp. 2091-2106, 2021/07/01 2021.

- [12] M. Pardo, E. R. Roberts, K. Pimentel, Y. A. Yildirim, B. Navarrete, P. Wang, *et al.*, "Size-dependent intranasal administration of magnetoelectric nanoparticles for targeted brain localization," *Nanomedicine: Nanotechnology, Biology and Medicine*, vol. 32, p. 102337, 2021/02/01/ 2021.
- [13] K. L. Kozielski, A. Jahansahi, H. B. Gilbert, Y. Yu, Ö. Erin, D. Francisco, *et al.*, "Nonresonant powering of injectable nanoelectrodes enables wireless deep brain stimulation in freely moving mice," *Science Advances*, vol. 7, p. eabc4189.
- [14] L. Carbone, C. Nobile, M. De Giorgi, F. D. Sala, G. Morello, P. Pompa, *et al.*, "Synthesis and micrometer-scale assembly of colloidal CdSe/CdS nanorods prepared by a seeded growth approach," *Nano Letters*, vol. 7, pp. 2942-2950, Oct 2007.
- [15] M. Baghbanzadeh, L. Carbone, P. D. Cozzoli, and C. O. Kappe, "Microwave-Assisted Synthesis of Colloidal Inorganic Nanocrystals," *Angewandte Chemie-International Edition*, vol. 50, pp. 11312-11359, 2011.
- [16] F. Ahmad, M. M. Salem-Bekhit, F. Khan, S. Alshehri, A. Khan, M. M. Ghoneim, *et al.* (2022, Unique Properties of Surface-Functionalized Nanoparticles for Bio-Application: Functionalization Mechanisms and Importance in Application. *Nanomaterials* 12(8).
- [17] R. Thirupathi, S. Mishra, M. Ganapathy, P. Padmanabhan, and B. Gulyás, "Nanoparticle Functionalization and Its Potentials for Molecular Imaging," *Advanced Science*, vol. 4, p. 1600279, 2017/03/01 2017.
- [18] R. Mout, D. F. Moyano, S. Rana, and V. M. Rotello, "Surface functionalization of nanoparticles for nanomedicine," *Chemical Society Reviews*, vol. 41, pp. 2539-2544, 2012.
- [19] V. Onesto, S. Forciniti, F. Alemanno, K. Narayanankutty, A. Chandra, S. Prasad, *et al.*, "Probing Single-Cell Fermentation Fluxes and Exchange Networks via pH-Sensing Hybrid Nanofibers," *ACS Nano*, vol. 17, pp. 3313-3323, 2023/02/28 2023.
- [20] F. Serio, N. Silvestri, S. Kumar Avugadda, G. E. P. Nucci, S. Nitti, V. Onesto, *et al.*, "Co-loading of doxorubicin and iron oxide nanocubes in polycaprolactone fibers for combining Magneto-Thermal and chemotherapeutic effects on cancer cells," *Journal of Colloid and Interface Science*, vol. 607, pp. 34-44, 2022/02/01/ 2022.
- [21] B. Tan, S. Gan, X. Wang, W. Liu, and X. Li, "Applications of 3D bioprinting in tissue engineering: advantages, deficiencies, improvements, and future perspectives," *Journal of Materials Chemistry B*, vol. 9, pp. 5385-5413, 2021.
- [22] R. Rizzo, V. Onesto, S. Forciniti, A. Chandra, S. Prasad, H. Luele, *et al.*, "A pH-sensor scaffold for mapping spatiotemporal gradients in three-dimensional in vitro tumour models," *Biosensors and Bioelectronics*, vol. 212, p. 114401, 2022/09/15/ 2022.
- [23] M. M. Vopson, Y. K. Fetisov, G. Caruntu, and G. Srinivasan. (2017, Measurement Techniques of the Magneto-Electric Coupling in Multiferroics. *Materials* 10(8).
- [24] A. Andolfi, P. Arnaldi, D. D. Lisa, S. Pepe, M. Frega, A. Fassio, *et al.*, "A micropatterned thermoplasmonic substrate for neuromodulation of in vitro neuronal networks," *Acta Biomaterialia*, vol. 158, pp. 281-291, 2023/03/01/ 2023.
- [25] A. Kaushik, J. Rodriguez, D. Rothen, V. Bhardwaj, R. D. Jayant, P. Pattany, *et al.*, "MRI-Guided, Noninvasive Delivery of Magneto-Electric Drug Nanocarriers to the Brain in a Nonhuman Primate," *ACS Applied Bio Materials*, vol. 2, pp. 4826-4836, 2019/11/18 2019.
- [26] Z. Ma, J. Mohapatra, K. Wei, J. P. Liu, and S. Sun, "Magnetic Nanoparticles: Synthesis, Anisotropy, and Applications," *Chemical Reviews*, 2021/12/30 2021.
- [27] S. Sun, H. Zeng, D. B. Robinson, S. Raoux, P. M. Rice, S. X. Wang, *et al.*, "Monodisperse MFe₂O₄ (M = Fe, Co, Mn) Nanoparticles," *Journal of the American Chemical Society*, vol. 126, pp. 273-279, 2004/01/01 2004.
- [28] K. Zhang, W. Zuo, Z. Wang, J. Liu, T. Li, B. Wang, *et al.*, "A simple route to CoFe₂O₄ nanoparticles with shape and size control and their tunable peroxidase-like activity," *RSC Advances*, vol. 5, pp. 10632-10640, 2015.
- [29] I. T. Smith, E. Zhang, Y. A. Yildirim, M. A. Campos, M. Abdel-Mottaleb, B. Yildirim, *et al.*, "Nanomedicine and nanobiotechnology applications of magnetoelectric nanoparticles," *WIREs Nanomedicine and Nanobiotechnology*, vol. 15, p. e1849, 2023/03/01 2023.
- [30] R. Guduru, P. Liang, C. Runowicz, M. Nair, V. Atluri, and S. Khizroev, "Magneto-electric nanoparticles to enable field-controlled high-specificity drug delivery to eradicate ovarian cancer cells," *Scientific reports*, vol. 3, pp. 2953-2953, 2013.
- [31] S. Betal, B. Shrestha, M. Dutta, L. F. Cotica, E. Khachatryan, K. Nash, *et al.*, "Magneto-elasto-electroporation (MEEP): In-vitro visualization and numerical characteristics," *Scientific Reports*, vol. 6, p. 32019, 2016/08/26 2016.

-
- [32] S. Betal, A. K. Saha, E. Ortega, M. Dutta, A. K. Ramasubramanian, A. S. Bhalla, *et al.*, "Core-shell magnetoelectric nanorobot – A remotely controlled probe for targeted cell manipulation," *Scientific Reports*, vol. 8, p. 1755, 2018/01/29 2018.
- [33] A. Kaushik, R. Nikkhah-Moshaie, R. Sinha, V. Bhardwaj, V. Atluri, R. D. Jayant, *et al.*, "Investigation of ac-magnetic field stimulated nanoelectroporation of magneto-electric nano-drug-carrier inside CNS cells," *Scientific Reports*, vol. 7, p. 45663, 2017/04/04 2017.
- [34] M. Nair, R. Guduru, P. Liang, J. Hong, V. Sagar, and S. Khizroev, "Externally controlled on-demand release of anti-HIV drug using magneto-electric nanoparticles as carriers," *Nature Communications*, vol. 4, p. 1707, 2013/04/16 2013.
- [35] S. Fiocchi, E. Chiamello, A. Marrella, G. Suarato, M. Bonato, M. Parazzini, *et al.*, "Modeling of core-shell magneto-electric nanoparticles for biomedical applications: Effect of composition, dimension, and magnetic field features on magnetoelectric response," *PLOS ONE*, vol. 17, p. e0274676, 2022.
- [36] N. A. García Saggió, P. S. Antonel, and F. V. Molina, "Magnetic and conducting composites of cobalt ferrite nanorods in a polyaniline matrix," *Polymer Engineering & Science*, vol. 60, pp. 597-606, 2020/03/01 2020.
- [37] S. Mushtaq, K. Shahzad, M. Rizwan, A. Ul-Hamid, B. H. Abbasi, W. Khalid, *et al.*, "Magnetoelectric core-shell CoFe₂O₄@BaTiO₃ nanorods: their role in drug delivery and effect on multidrug resistance pump activity in vitro," *RSC Advances*, vol. 12, pp. 24958-24979, 2022.
- [38] K. Raidongia, A. Nag, A. Sundaresan, and C. N. R. Rao, "Multiferroic and magnetoelectric properties of core-shell CoFe₂O₄@BaTiO₃ nanocomposites," *Applied Physics Letters*, vol. 97, p. 062904, 2010.
- [39] J.-C. Si, Y. Xing, M.-L. Peng, C. Zhang, N. Buske, C. Chen, *et al.*, "Solvochemical synthesis of tunable iron oxide nanorods and their transfer from organic phase to water phase," *CrystEngComm*, vol. 16, pp. 512-516, 2014.
- [40] A. Marrella, G. Suarato, S. Fiocchi, E. Chiamello, M. Bonato, M. Parazzini, *et al.*, "Magnetoelectric nanoparticles shape modulates their electrical output," *Frontiers in Bioengineering and Biotechnology*, vol. 11, 2023.